The Diurnal Cycle of Clouds and Precipitation at the ARM SGP Site

Wei Zhao

A thesis

submitted in partial fulfillment of the

requirements for the degree of

Master of Science

University of Washington

2017

Committee:

Roger T. Marchand

Qiang Fu

Christopher S. Bretherton

Program Authorized to Offer Degree:

Atmospheric Sciences

University of Washington

Abstract

The Diurnal Cycle of Clouds and Precipitation at the ARM SGP Site

Wei Zhao

Chair of the Supervisory Committee:
Professor Roger T. Marchand
&
Professor Qiang Fu
Department of Atmospheric Sciences

Millimeter Wavelength Cloud Radar (MMCR) data from Dec. 1996 to Dec. 2010, collected at the U. S. Department of Energy (DOE) Atmospheric Radiation Measurement (ARM) program Southern Great Plains (SGP) site are used to examine the diurnal cycle of hydrometeor occurrence. These data are categorized into clouds (-40 dBZe ≤ reflectivity < -10 dBZe), drizzle and light precipitation (-10 dBZe ≤ reflectivity < 10 dBZe), and heavy precipitation (reflectivity ≥ 10dBZe). The same criteria are implemented for the observation-equivalent reflectivity calculated by feeding outputs from a Multiscale Modeling Framework (MMF) climate model into a radar simulator. The MMF model consists of the NCAR Community Atmosphere Model (CAM) with conventional cloud parameterizations replaced by a cloud resolving model (CRM). The annual and seasonal mean composites between observations and the model are compared.

Meanwhile, a set of atmospheric states that were created specifically for the ARM Southern Great Plains (SGP) site by Evans et al. [2017] are used to investigate in which atmospheric state or states the MMF does well or poorly. Differences (or errors) in the annual diurnal cycle between observations and the MMF model are decomposed into differences due to the relative frequency of occurrence of states, the daily-mean vertical profile of hydrometeor occurrence and the (normalized) diurnal variation of hydrometers in each state.

The results show that a radar simulator combined with the simple reflectivity categories can be an effective approach for evaluating diurnal variations in model hydrometeor occurrence. Based upon the comparison, the MMF only marginally captures observed increases in the occurrence of boundary layer clouds after sunrise in spring and autumn, and does not capture diurnal changes in boundary layer clouds during the summer. Above the boundary layer, the MMF captures reasonably well diurnal variations in the vertical structure of clouds, light and heavy precipitation in the summer but not in the spring. The state-wise analysis shows that the model underestimates boundary layer clouds but overestimates high clouds and precipitation in almost all the states. In terms of the diurnal variation, the MMF does not capture that of low clouds in any state, but does a reasonable job capturing the diurnal variation of high clouds and precipitation in summer states though not in those states which occur in the transition seasons (spring and fall). Overall, the error in individual states and in the annual composite is due primarily to error in the daily mean of hydrometeor occurrence (rather than the diurnal variations). However, errors in the state frequency (that is the distribution of weather states in the model) also play a significant role.

TABLE OF CONTENTS

LIST OF FIGURES

LIST OF TABLES

Table Number Page

Acknowledgment

First of all, I would like to express my greatest gratitude to my advisors Roger Marchand and Qiang Fu for inspiring and guiding me patiently along the way. They are extremely supportive and encourage me to explore. It is a fun experience to sit between advisors every time we have a meeting together because sometimes they two will argue with each other and I do learn a lot from it. I am also grateful to Christopher Bretherton for serving as my committee and providing valuable comments. Thanks to Tom Ackerman for all the suggestions. Finally, I would like to thank my dear grads14, Chinese student associate, Qiang's group, Roger and Tom's group for all the support.

Chapter 1 : Introduction

The diurnal cycle of clouds and precipitation has strong impacts on the Earth radiative budget via interactions with solar and longwave radiation [Bergman and Salby, 1997], and on the hydrological cycle through evaporation and runoff [Dai et al., 2004]. For instance, given the same temperature and moisture vertical profile, a cloudy night will be warmer at the surface than its cloud-free counterpart because clouds will trap the outgoing longwave radiation in the atmosphere. Meanwhile, only clouds that occur during the day can reflect sunlight back into space. Also, precipitation tends to be evaporated faster during daytime than nighttime because solar radiation provides energy for evaporation; and this changes the fraction of runoff versus evaporation, as well as the surface latent and sensible heat fluxes [Dai et al., 2004]. A good knowledge of the diurnal cycle of clouds and precipitation is also of vital importance in developing strategies to utilize rainfall or solar energy [Easterling and Robinson, 1985].

Observational studies on the diurnal cycle of precipitation have shown that there is a preferential timing or phase for the maximum occurrence of precipitation that varies from one place to another and from season to season [Wallace, 1975; Dai et al., 1999; Liu and Zipster, 2008; Nesbitt et al., 2008]. Wallace [1975] used hourly data on the frequencies of all types of precipitation events from more than 100 stations in the United States and discovered that there is a nocturnal to early morning precipitation occurrence maximum over the U.S. Southern Great Plains (SGP) in summer. Easterling and Robinson [1985] using a 25-year record of thunderstorms from 450 stations in the conterminous United States, likewise found the majority of thunderstorms occur at night during summer in this area. Diurnal variation of precipitation occurrence in other seasons at SGP is much weaker but with some evidence for a weak early to

late morning maxima in the winter [Wallace, 1975; Dai et al., 1999]. Comparisons between observations and climate model simulations of the diurnal cycle of surface precipitation over land have been intensely investigated in different parts around the globe. These studies indicate that conventional GCMs tend to precipitate too frequently and too early during the day [e.g., Dai et al., 1999; Collier and Bowman, 2004; Dai, 2006; Lee et al., 2010; Stephens et al., 2010; Covey et al., 2016]. Even with a resolution as high as 0.25 degree in latitude-longitude, climate models used in Covey et al. [2016] still find similar problems which is, to large extent, thought to be due to the subgrid physics represented by the model cumulus parameterization schemes.

As regards the diurnal cycle of clouds, Dong et al. [2006] showed that, in the annual mean, low clouds occur more often during daytime while the occurrence of both middle and high clouds is relatively invariant. Whereas in the warm season high clouds occur more often between late afternoon and the following morning [Zhang and Klein, 2010]. Given the difficulty that GCMs have in capturing the correct timing of precipitation (and the transition from shallow convection to deep convection), it is not surprising that GCMs generally struggle to capture the diurnal cycle of both high clouds and low clouds [Tian et al., 2004; Dai and Trenberth, 2004; Jiang et al., 2015;]. Lin et al. [2015] showed that even when using large scale forcing derived from observation at SGP to drive the single-column Community Atmosphere Model version 5 (SCAM5), this model often lacked shallow cumulus clouds and tended to over represent deep convection.

The inability of GCMs to correctly predict the diurnal cycle of clouds and precipitation indicates missing or poorly represented mechanisms driving them, and this may distort longer timescale variability and degrade future projections [Dai et al., 2004; Pritchard et al., 2009b]. Under climate scenarios with increased CO_2, it is broadly expected that the land surface will warm, wet

areas will get wetter and dry areas drier in the mid to high latitudes, and more moisture will be transported into the storm tracks [Trenberth, 2011]. A study by Jiang et al. [2016] using an ensemble of regional climate models (RCMs) suggests that storms in most regions of the United States will have shorter duration and larger average intensity in the future. It is specifically predicted for SGP that there will be less precipitation and more drought events, which will harm local agricultural productivity [Shafer et al., 2014]. These expectations suggest that correctly capturing the diurnal cycle of clouds and precipitation will become increasingly important in modeling and understanding regional climate change impacts for the SGP and much of the United States.

In this thesis, we examine the characteristics of the diurnal cycle of clouds and precipitation for the SGP with an emphasis on vertical structure, and evaluate the ability of a Multiscale Model Framework (MMF) climate simulation to reproduce these features. Specifically, we use observations from the Atmospheric Radiation Measurement (ARM) program vertically-pointing cloud radar at its SGP site and compare these observations with the MMF simulations, following the radar simulator approach used by Marchand et al. [2009a, 2009b]. MMFs, also known as superparameterization (SP), have been developed largely to avoid difficulties related to cumulus parameterization in conventional GCMs. They are GCMs with a two-dimensional or small three-dimensional cloud resolving model (CRM) embedded into each GCM grid cell [Randall et al., 2003]. Nominally, MMFs can explicitly simulate deep convection, fractional cloudiness, cloud overlap, and the spatial distribution of precipitation intensity [Randall et al., 2003].

Khairoutdinov et al. [2005] compared the diurnal cycle of precipitation from the NCAR Community Atmosphere Model (CAM) and superparameterized CAM (SP-CAM). They found that the diurnal variability of precipitation frequency over land is dramatically improved in the

SP-CAM. Similarly, Pritchard and Somerville [2009a] and Pritchard et al. [2011] demonstrated an overall improvement in the diurnal cycle of precipitation during summer in their MMF simulations relative to a conventional GCM. Zhang et al. [2008] examined the diurnal cycle of precipitation, high altitude cloud, and upper tropospheric humidity over the tropics. They found that the MMF does capture the diurnal timing of all three quantities over tropical land, though perhaps with an amplitude that is too small.

Our objectives are, first to identify what diurnal variations are evident in annual and seasonal composites of the ARM MMCR radar reflectivity profile measurements from the SGP. Based on previous work by Zhang and Klein [2010] among others, one expects that (at least) during the summer season, there are significant diurnal variations. We group the hydrometeors into three categories, specifically, cloud, drizzle and light precipitation, and heavy precipitation based upon their reflectivity and examine the frequency of occurrence of each category. Key features in the diurnal cycle of these categories are identified. Additional details on the data and methodology are given in chapter 2. Our second objective is to evaluate the degree to which a cloud radar-simulator in combination with the reflectivity categories might be useful in evaluating climate models, and potentially other models. A radar simulator [Haynes et al., 2007] is already embedded into the Cloud Feedback Model Intercomparison Project (CFMIP) Observations Simulator Pack (COSP), which is being used by many climate modeling centers [Bodas-Salcedo et al., 2011]. While this simulator is used primarily to simulated NASA CloudSat radar reflectivities (meaning a downward looking 94 GHz system), it can and has been used to simulate ARM radar reflectivities [Marchand et al., 2009b]. Output diagnostics may well be added to the COSP simulator package to facilitate comparison between ARM radar datasets and climate models. A development version of this code is currently available from COSP repository

[Zhang et al., 2017]. Our third objective is to further previous investigations of the MMF diurnal cycle over land, and in particular we focus here on the vertical structure of hydrometeor occurrence. These first three objectives are undertaken in Chapter 3.

In chapter 4, we expand upon our study in chapter 3 using an atmospheric-state based compositing approach. A set of atmospheric states are adopted that were created specifically for the ARM Southern Great Plains (SGP) site by Evans et al. [2017] following an earlier approach developed by Marchand et al [2009b]. A brief description of the classification approach and resulting atmospheric states is provided in chapter 2. This approach also enables us to decompose differences (or errors) in the annual diurnal cycle between observations and the MMF model into differences due to the relative frequency of occurrence of states, the daily-mean vertical profile of hydrometeor occurrence and the (normalized) diurnal variation of hydrometers in each state. While we show and discuss mean model biases, our primary focus in chapter 4 is evaluating the diurnal variations. Our expectation (or hypothesis) at the start of this investigation was that MMF would not capture the diurnal variation well in all states, and indeed, we will show that this is the case. More broadly, our objectives in chapter 4 are (1) to find in which atmospheric state or states the MMF does well or poorly (with an expectation that this will give us insights into the cause of underlying problems) and (2) to determine if the relative frequency of states contributes significantly to errors in annual diurnal cycle of cloud and precipitation occurrence.

In Chapter 5, ECMWF interim reanalysis [Dee et al., 2011] and ARM SGP surface measurement are used to explore potential reasons of the differences between the radar observations and the MMF. Finally, the conclusions are summarized in the end.

Chapter 2 : Data and Methodology

2.1. ARM radar observations

The ARM program Active Remote Sensing of Clouds (ARSCL) Value-Added Product (VAP) for the SGP site is used in this study (**DOI**: 10.5439/1027282). This data product combines measurements from a Vaisala ceilometer, micropulse lidar and millimeter cloud radar (MMCR) [Clothiaux et al., 2000]. The ARM MMCR is a vertically-pointing 35GHz system [Moran, 1998]. It is able to penetrate clouds and most rain and produces range resolved measurements of hydrometeor reflectivity using a variety of operation modes, with vertical resolutions varying between about 45 and 90 m, and with dwell (or integration) times of a few seconds [Clothiaux et al., 2000]. The only variable analyzed in this study is the best-estimate reflectivity data selected by ARSCL from the available operating modes of MMCR. It has a fixed time-height grid with a temporal sampling of 10 s and a spatial sampling of 45 m. However, the radar hydrometeor detection (the so called cloud or hydrometeor mask) does utilize lidar data to assist in discriminating between hydrometeors and clutter (generally insects). The MMCR at SGP was operated nearly continually from Dec. 1996 to Dec. 2010 and thus provides a fairly long data record to explore the climatology of hydrometeor occurrence. Only 11.4% of the best-estimate reflectivity data are missing or are known to be low quality such that they are not used. However, the calibration of the MMCR was not routinely checked against external targets [Kollias et al. 2016]. We discuss this issue further, later in this section.

2.2. MMF model

The MMF model outputs used in this study were generated as detailed in Marchand et al. [2009a], and we only introduce it briefly here. The host model, CAM (version 3.0), has 26

vertical layers and its horizontal resolution is 2º×2.5º. The model was run with the finite-volume dynamical core using a dynamical time step of 20 min. In the MMF configuration, the diagnostic cumulus parameterization and other cloud schemes [Collins et al., 2006] are replaced by a CRM which is the System for Atmospheric Modeling (SAM) [Khairoutdinov and Randall, 2003]. In each grid cell, SAM is oriented east-west and has 64 columns with 4 km horizontal resolution and cyclic lateral boundary conditions. Independent of the dynamical time step of CAM, SAM is run with a much higher time resolution of 10 to 15 s. Radiative heating is calculated within CAM every 10 min. The MMF run was initialized on 1 Sep. 1997 and stopped on Jun. 2002 and was forced using observed monthly sea-surface temperature. Taking model spin-up into consideration, only data from Aug.1998 to Jun. 2002 are used in this analysis.

Instead of converting radar observations to condensate mixing ratios or other 'model-equivalents' (with inherently large uncertainties), we forward calculate radar reflectivity, an 'observation-equivalent', by feeding outputs (mixing ratios) from the MMF model into a radar simulator. The details of the forward calculation are the same as in Marchand et al. [2009a], except that instead of mimicking the CloudSat radar, looking downward from space at 94 GHz, we do so for the ARM MMCR, which looks upward at 35 GHz. This simulator accounts for attenuation caused by particles and gases. It treats all the particles as equivalent-volume spheres and uses Mie theory to calculate scattering and attenuation. The particle size distributions and particles densities (for all model hydrometeor types) are consistent with the model microphysical scheme [Marchand et al. 2009a]. To speed up computations, look up tables are used and designed to keep errors within 1.2 dBZe as compared to the full Mie calculations. Meanwhile, multiple scattering effects are ignored. To be consistent, the simulator uses the same particle

size distribution as in the MMF. The simulated reflectivity data represent snapshots in time with one snapshot every 3 hour at a vertical resolution of 480 m.

2.3. Atmospheric States

The radar data mentioned above are sorted into different atmospheric states previously identified using a neutral network classifier by Evans et al [2017]. The classifier uses ERA-Interim state variables (horizontal winds, relative humidity, temperature at seven predetermined pressure level and surface pressure; Dee et al., 2011) on a 9×9 grid with 1.5º×1.5º spatial resolution centered on the SGP site. In the state classification process, ARM radar observations are utilized to ensure cloud properties in each state are temporally stable and statistically different from those in other states [Marchand et al. 2009b, Evans et al. 2017]. There are totally 21 states defined by the classifier and the outputs from it are (1) a time series indicating to which of the 21 atmospheric states found by Evans, the atmosphere most closely resembles (the time interval is 6 hours following from the availability of ERA-Interim variables) and (2) a definition of each atmospheric state, which mathematically is a set of vectors representing specific synoptic conditions. As an example, Figure 2.1 shows the surface pressure anomaly and 875 hpa winds (upper panel) and 500 hpa relative humidity and winds (bottom panel) of state 4, 8, 19, 20 and 21 centered over SGP. State 4 has a high pressure to the east and a low pressure to the northwest of the domain with southward winds at surface and southwesterlies at 500 hpa. These indicate the existence of a cold front which is still far away and the SGP is likely in the warm sector. State 8 shows a cold front in the domain as illustrated by the deep low over SGP and the changes of wind direction from northerlies to southwesterlies. State 19, 20, and 21 occurs most frequently in summer and all have the typical low level southerlies. State 19 has a cyclonic flow at 500 hpa while state 20 and 21 show westerlies. Of the three states, state 20 is the wettest with largest

relative humidity at 500 hpa and state 21 has a negative surface pressure anomaly over the domain with a convergence zone to the northwest of the SGP. Different large forcing configurations lead to different characteristics of diurnal cycle of clouds and precipitation which will be discussed later in this article. More complete descriptions of these atmospheric states can be found in Evans et al. [2017].

2.4. Decomposition of Differences

We explore the differences between the observed and simulated annual diurnal cycle of cloud and precipitation occurrence. To accomplish this, in chapter 4, we represent the observed (or modeled) annual diurnal cycle as a sum of contributions from each atmospheric state. We then further decompose the contribution from each state into a daily-mean profile (or intensity) and a diurnal-variation. Mathematically,

$$(HO_t)_{obs} = \sum_{i=1}^{N}(HO_{i,t})_{obs} * (SF_{i,t})_{obs} = \sum_{i=1}^{N}\overline{(HO_i)_{obs}} * (HO_{i,t})'_{obs} * (SF_{i,t})_{obs} \quad (1)$$

$$(HO_t)_{mod} = \sum_{i=1}^{N}(HO_{i,t})_{mod} * (SF_{i,t})_{mod} = \sum_{i=1}^{N}\overline{(HO_i)_{mod}} * (HO_{i,t})'_{mod} * (SF_{i,t})_{mod} \quad (2)$$

where $(HO_t)_{obs}$ represents the observed hydrometeor occurrence profile at hour t (t=0, 1, … , 23) in the annual mean, $(HO_{i,t})_{obs}$ is the hydrometeor occurrence profile at the same hour in the *i*-th state (i=1, 2, …, 21) and $(SF_{i,t})_{obs}$ is the frequency of *i*-th state for the same hour. $(HO_{i,t})_{obs}$ can be further written as the daily mean (mean over hour t) $\overline{(HO_i)_{obs}}$ multiplied by $(HO_{i,t})'_{obs}$ which represents daily-mean hydrometeor occurrence profile of the *i*-th state and the normalized diurnal variations, respectively. Equation (2) is the same as equation (1) except applied to the model (with subscript of mod).

Note that the frequency of occurrence of the states can vary with time of day (e.g. one might tend to be in state 1 more often at 10 am than 10 pm) and consequently $(SF_{i,t})_{obs}$ is a function of

time. In principle one could decompose the frequency term into a daily mean and diurnal variation, however, differences due to the diurnal frequency variations are small and we opt not to introduce this additional complexity. Rather, the terms $(HO_{i,t})'_{obs}$ and $(HO_{i,t})'_{mod}$ capture the normalized diurnal variation of hydrometeor occurrence for both observations and model simulations, respectively, and our primary objective, in some sense, is to determine how similar these terms are.

In chapter 3, we examine the vertical structure of the diurnal cycle of hydrometeor occurrence using three reflectivity ranges. For simplicity we will call reflectivity values between -40 and -10 dBZe "cloud", from -10 to 10 dBZe "drizzle and light precipitation" and values larger than 10 dBZe "heavy precipitation", though we recognize that radar volumes with reflectivity values less than -10 dBZe do at times contain particles which are large enough to be called drizzle or potentially even rain. To better describe the vertical structure, we divide the troposphere into boundary layer (below 2.5 km), middle troposphere (2.5-7.5 km) and upper troposphere (above 7.5 km), based on the altitude above ground level.

For both observations and model outputs, the hourly mean occurrence rate for each category is first produced at every vertical level and then, the annual and seasonal diurnal cycle is composited. Two aspects of the composites are analyzed. One is the daily mean hydrometeor occurrence (which will be discussed in terms of boundary layer, middle and upper troposphere averages). And the other is the diurnal variation or timing that is evaluated using a moving-bootstrap method [Marchand et al., 2006]. This method identifies if the hydrometeor occurrence at a given time and vertical level is significantly larger or smaller than the daily mean for that vertical level, with a 95% confidence. Our goal is to determine when the observed variations are

large enough to be statistically significant and identify broadly the timing (or phase) of key features in the observations.

For simplicity, in chapter 4, the hydrometeors are classified into only two categories which are clouds (-40 dBZe ≤ reflectivity < -10 dBZe) and precipitation (reflectivity ≥ -10 dBZe). We first look at the annual diurnal cycle of clouds and precipitation for both observations and simulations, and then decompose them into 21 atmospheric states to see the performances of the MMF given similar meteorological conditions. Finally, by means of equations (1) and (2), we examine what terms contributes most to the differences between observations and simulations in the annual diurnal cycle of cloud and precipitation occurrence.

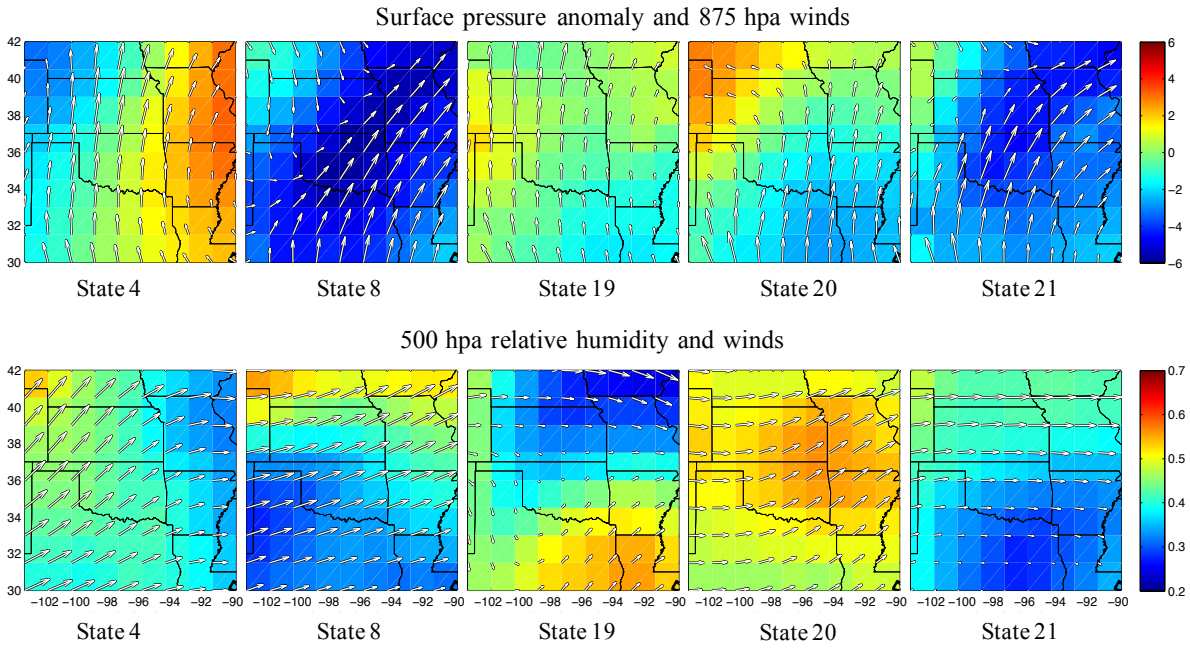

Figure 2.1 Large scale forcing configurations of state 4, 8, 19, 20 and 21. Upper panel shows surface pressure anomaly and 875 hpa winds averaging from Dec. 1996 to Dec. 2010 using ECMWF reanalysis data. Bottom panel shows 500 hpa relative humidity and winds. Detailed description of these states can be found in the main text.

Chapter 3 : Annual and seasonal cycle

3.1. Diurnal cycle of hydrometeors in MMF simulations

In this section we present and discuss results showing the composite diurnal cycle of hydrometeor occurrence. For discussion purposes, we divide the troposphere into boundary layer (below 2.5 km), middle troposphere (2.5 – 7.5 km) and upper troposphere (above 7.5 km), based on the altitude above ground level and we organize the discussion into 5 themes: boundary layer clouds, high clouds and middle clouds, drizzle and light precipitation, heavy precipitation, and the combination of all the hydrometeors. For each theme we begin the discussion with an examination of the annual composite, and then discuss how it varies with season. As explained in more detail below, particular attention is also paid to the sampling uncertainty.

Figure 3.1 shows the annual diurnal cycle of occurrence at SGP for (a) clouds, (b) drizzle and light precipitation, (c) heavy precipitation and (d) the combination with 1 hour temporal and 45 m vertical resolutions, based on the ~14 year ARSCL dataset. The time is local (UTC time minus 6 hour) and the color denotes the occurrence percentage, calculated by dividing the number of samples that fit into each category in each hour by the total number of samples for that hour and multiplying by 100. Note that the occurrence percentage is calculated with respect to a specific altitude bin (and is not the vertically projected cloud area that is much larger because clouds at each vertical level are not always maximally overlapped). Also note that a different scale is used in each panel of Fig.3.1.

3.1.1. Boundary Layer Clouds

Boundary layer clouds in the annual composite (Fig.3.1a) have a daily average occurrence rate of 5.8%. This value is calculated by averaging the diurnal mean occurrence at all altitudes that belong to boundary layer (taken here as altitudes below 2.5 km). The results for other categories and layers are presented in Table 3.1. Boundary layer clouds exhibit a diurnal variation where clouds are most plentiful between 6 am and early afternoon and cloud top tends to increase in altitude starting around 6 am and reaching a maximum of about 2.5 km at 4 pm local time. Their occurrence and height decrease rapidly between 4 and 6 pm with a minimum in occurrence between 6 and 8 pm local time.

The moving-bootstrap method mentioned above has been used to determine whether the cloud occurrence at a given time and at a given altitude is significantly larger or smaller than the daily mean value at the same altitude. Figure 3.2 shows the significance-test results for various hydrometeors in the annual composite. Red indicates that the frequency is significantly larger than the daily mean at the same altitude (at the 95% level of confidence), blue represents significantly smaller, and white shows the deviation from the mean is not significant.

Figure 3.2a indicates that diurnal variation in the occurrence of boundary layer clouds is significant (meaning that this unlikely is a result of sampling uncertainty), as is the cloud lifting, and timing variations discussed above. Except where stated otherwise, all the diurnal features discussed in this section are likewise significant at the 95% level of confidence. These boundary layer diurnal characteristics are present to varying degrees in spring, summer and fall seasons as shown in Fig.3.3a. In winter, on the other hand, the boundary layer clouds are located at lower altitudes, and have no discernable change in cloud top height. There is a slight increase in cloud

occurrence between 6 am and early afternoon, with the value reaching 10 - 12% between 7 am to 3 pm and 6 - 10% for the rest of the day. However, this change in occurrence in winter is not significant at the 95% level of confidence (Fig.3.4a). The mean (daily) average of occurrence (between 0 and 2.5 km) in winter, spring, summer and autumn is 6.7%, 7.3%, 3.6% and 5.1%, respectively (Table 3.1) (Again we stress that this is not the vertically projected area, but a volume average, the mean occurrence of cloud at all altitudes, between 0 and 2.5 km). This result is consistent with Lazarus et al. [2000], who found that low cloud amounts are larger in spring and winter and smaller in summer and autumn in the evaluation of Observer/Edited Cloud Reports, Micropulse Lidar and Belfort Ceilometer cloud detections, and ISCCP satellite retrievals for the SGP.

The diurnal variation of boundary layer clouds in spring, summer and fall at SGP is mainly driven by solar warming of the surface. This warming produces an absolutely buoyantly unstable layer near the surface which then becomes the source of buoyant air parcels that generates turbulence, entrains warm, dry free-tropospheric air into boundary layer and leads to the formation of the daytime convective boundary layer clouds [Angevine et al., 2001]. The availability (including advection) of moisture in the boundary layer also plays a central role, controlling whether the boundary layer clouds will remain shallow or transition to deeper precipitating clouds [Zhang and Klein, 2010]. Besides these factors, surface wind speed and free tropospheric humidity are known to affect low cloud amounts as well [Stevens and Brenguier, 2009; Kuang and Bretherton, 2006].

3.1.2. High and Mid-Level Clouds

In the annual composite (Fig.3.1a), the daily average of high cloud occurrence is 7.6% (Table 3.1). Note that this value is calculated using height bins between 7.5 and 12.5 km, since above 12.5 km cloud occurrence is quite small. The same height range is used for all other upper level hydrometeors in Table 3.1. Most of the high cloud is concentrated between 7.5 and 10.5 km with an occurrence of 10 - 12% (Fig.3.1a). The small diurnal variation in this height range (with a bit more high cloud after 6 pm local time than between 9 am and 6 pm), evident in Fig.3.1a, is not significant (Fig.3.2a) which is consistent with the result reported by Dong et al. [2006] in the annual mean. However, the variations in (the relatively small amount of) cloud around 12.5 km (in the annual) mean is significant. This variation is due primarily to diurnal variation in the spring and summer. Figure 3.3a shows the peak in high cloud occurrence in spring and summer is both higher in altitude (10 to 12.5 km in summer) and contains significant diurnal variations at the 95% level of confidence (strongest in summer) (Fig.3.4a). In spring there is more high cloud between 7 and 11 km (meaning a greater occurrence of the highest cloud) in the late afternoon and evening than in the early morning hours. In summer, the peak in high clouds occurs during night and extends into morning hours (decreasing noticeable after 5 or 6 am) as well as being somewhat higher in altitude (between 10 and 12.5) than the spring. While the smaller diurnal variations in high cloud occurrence seen in autumn and winter may be real, they are not significant at the 95% level of confidence and could be a result of sampling uncertainty.

The weak diurnal variation in cloud occurrence in upper and middle troposphere in the winter is not surprising given that these clouds are mainly produced by large scale forcing (frontal systems), which have little if any preferred diurnal timing. The strong variations in summer high cloud are generated by convection, which is often initiated by solar heating of the surface

(though not necessarily locally; Carbone et al., 2002), and as will become clearer in the following sections, tends to begin predominately in the late afternoon or evening [Jiang et al., 2006; Lee et al., 2010]. In the transition seasons (spring and autumn) both frontal systems (with little diurnal preference) and diurnally driven convection likely contribute.

The occurrence of mid-level clouds is smaller than both boundary layer clouds and high clouds, with a mean occurrence (volume average) of only 2 - 6%. Their diurnal variations are weak compared to boundary layer clouds, with a peak occurrence between 3 and 9 am in the annual composite. This is due primarily to diurnal variation in the summer, which is the only season in which the diurnal variation is clearly significant at mid-levels (Fig.3.4a) and is associated with a peak in light precipitation that occurs at this same time of day, as is discuss in the next two subsections.

3.1.3. Drizzle and Light Precipitation

Drizzle and light precipitation is concentrated in the middle troposphere and below about 1 km in the annual composite (Fig.3.1b). Of course, much of the light precipitation above the boundary layer is ice and we are not distinguishing between cases where there are few-but-large or many-but-small particles present in the radar volume. Here we are identifying light precipitation solely based on a 35 GHz reflectivity between -10 and 10 dBZe. For water clouds in and near the boundary layer, a reflectivity above -10 dBZe is indicative of having drops that are at least drizzle-sized (diameters greater than 50 um) [Frisch et al., 1995; Mace and Sassen, 2000; Liu et al., 2008]. For ice clouds, there is perhaps a less clear distinction between what constitutes "precipitating" rather than "cloud" ice. Nonetheless, reflectivity values greater than -10 dBZe are indicative of having particles that are large enough to have appreciable fall velocities. We

stress that in either case (liquid or ice phase) these volumes will also often contain cloud size particles (diameters smaller than 50 um) but we can not determine this from the radar reflectivity alone. It is noteworthy that light precipitation is almost as frequent as cloud in the middle troposphere. This suggests that many of the hydrometeors in the middle troposphere at SGP are either falling from higher in the atmosphere or are associated with a recent or active updraft (for example, as part of a cumulus congestus) and contain larger precipitating particles. A potentially important caveat here is that altostratus or altocumulus composed entirely of small liquid droplets can have a reflectivity below the ability of the ARM MMCR to detect them. However, comparison of the MMCR radar detections against lidar (which can easily detect these altostratus and altocumulus) shows the radar is missing only a small percentage of clouds that are detected by the lidar in this height range (at least when the lidar is not blocked by low level clouds) [Clothiaux et al., 2000]. Thus, while the cloud occurrence may be underestimated slightly, it is likely that reflectivity values greater than -10 dBZe contribute substantially to the reflectivity distribution at mid-levels at SGP.

Overall, Fig.3.1b shows a minimum occurrence between noon and 6 pm, with a peak occurrence of 5 - 8% between 4 and 8 am near 4 - 6 km. While there are distinct differences in the occurrence rates and the vertical distributions, all four seasons (Fig.3.3b) show the same general pattern with a minimum between about noon and 6 pm (in both the middle troposphere and near the surface). However, only in summer is this pattern clearly significant at the 95% level of confidence throughout the troposphere (Fig.3.4b). Summer also features a wider minimum (starting closer to 10 am), and a peak near-surface occurrence rate overnight (0 to 6 am). The timing of this overnight peak is to large extent consistent with that found in Wallace [1975] for surface precipitation during the summer. In the upper troposphere in spring and summer, there is

greater occurrence of precipitating particles between 8 and 12.5 km in the evening, after which time the frequency of occurrence in the upper troposphere decreases slowly into the early morning hours and shifts towards lower altitudes (Fig.3.3b). The diurnal variations for these high-altitude hydrometeors are statistically significant at the 95% level of confidence in both seasons, but the variation in the middle troposphere is not significant in spring (Fig.3.4b), perhaps because the there is more light precipitation during the daytime minimum in spring as compared to summer. As in the discussion of high clouds, we speculate that this is because the spring seasonal composite has a significant contribution from frontal systems that have little preferred diurnal timing. The diurnal variations in winter and autumn display little if any change in the highest altitudes occupied by light precipitation; and while there are some increases in light precipitation in the late evening and early morning in the winter, this diurnal variation is not clearly significant (and could be due to sampling uncertainty).

3.1.4. Heavy Precipitation

Heavy precipitation occurs much less frequently than clouds or light precipitation, with the largest frequencies being about 1.5 - 2% in the annual composite (Fig.3.1c), so the sampling uncertainty is notably higher. Fig.3.1c also shows heavy precipitation is mainly below 10 km with peak occurrence rates between 1 - 2 km during early morning and evening, though only the early morning peak is significantly larger than the daily mean (Fig.3.2c). In spring, precipitation near the surface occurs mainly in the evening with a frequency of 2 - 2.5%, while the frequency in the early morning is somewhat smaller (Fig.3.3c). The opposite is true in the summer where precipitation near the surface is most frequent in the early morning (again with a frequency of about 2 - 2.5%). Higher in the atmosphere, there is a peak between 4 - 7 km during the evening in spring, and in the case of summer, peaks exist between about 6 - 10 km during the evening

and between 5 - 7 km during early morning (following and a bit lower in altitude than peaks in the light precipitation category) all of which are statistically significant (Fig.3.4c). For winter and autumn, most the precipitation is concentrated below 5 km and 3 km, respectively with a frequency of 1 - 2%. While there may be some increases in heavy precipitation occurrence in the winter between 8 am and 3 pm, the change is not significant.

The diurnal variations of heavy precipitation in summer that are found here, agree with the results of Wallace [1975] for summer, and show spring (in the aggregate) follows a similar pattern. Of course, our results are not constrained to the surface, but also show the vertical structure of the diurnal variations. Examining the time-space coherence of precipitation patterns using Weather Surveillance Radar data, Carbone et al. [2002] found that this nocturnal precipitation maximum was connected with the passage of eastward-propagating rainfall systems, most of which were mesoscale convective systems (MCSs) originating near the Continental Divide. These systems mainly happen during the warm season (April to September) [Fritsch et al., 1986] and tend to pass over the SGP most often between May and August. These systems have more complicated dynamics than a single cumulonimbus with larger and higher cirriform anvil clouds, larger stratiform precipitating areas, and longer durations [Houze et al., 2004]. Local deep convection tends to be vigorous during spring and summer in the late afternoon or night because of the strong surface solar heating during the day, strong transport of moisture by low level jet at night, and a reversal of the region mountain-plain circulation [Carbone and Tuttle, 2008]. Due to vigorous convection and MCSs, the height that both clouds and precipitation reach is higher during evening and early morning in spring and summer, as observed in the diurnal patterns for all of our categories (cloud, light and heavy precipitation).

3.1.5. All Hydrometeors

When all the hydrometeors are considered (Figs. 3.1d and 3.3d), their annual and seasonal diurnal cycles combine the main characteristics of those of clouds and precipitation discussed above. Some characteristics become clearer. For example, the increased occurrence and lifting of boundary layer hydrometeors after 6 am becomes clearer in combination, because hydrometeors we have classified as both cloud and precipitation contribute. In winter (Fig.3.3d), in particular, boundary layer hydrometeors occurrence (especially the slight increase in occurrence between 8 am and noon) is due roughly equally to clouds (low reflectivities) and drizzle (moderate reflectivities – which may include both cloud and drizzle). Likewise, the strong diurnal cycle of high clouds and high-altitude precipitation in the spring and summer is clearer when compositing all hydrometeors, again because cloud and precipitation covary. In particular, the sharper evening peak in spring (as compared to the broader maximum in summer) is better captured in Fig.3.3d than in 3.3a. On the other hand, some features are difficult to see when compositing all hydrometers. In particular, the tendency for both heavy and light near-surface precipitation to be greater overnight and in the early morning in summer, but greater in the evening in spring is difficult to see in the composite including all hydrometeors. This is because the occurrence of precipitation is generally smaller than clouds.

We conclude this section noting that the ARM cloud radar is clearly able to capture a variety of diurnal variations in vertical structure of hydrometeor occurrence. Furthermore, an evaluation using simple reflectivity thresholds that separate (to a degree) cloud, light and heavy precipitation (while far from perfect) is useful in understanding the diurnal variations. We summarize a variety of key features, which are discussed in this section, in Table 3.2. In the

following section, we evaluate the degree to which an MMF model simulation was able to capture these features.

3.2. Diurnal cycle of hydrometeors in MMF simulations

Here we compare MMF outputs with the observed radar composites presented in the previous section, with a particular focus on the key features of the diurnal cycle summarized in Table 3.2. We discuss the possible causes of the differences between model and observations in chapter 5. Figures 3.5 and 3.7 are the same as Figures 3.1 and 3.3, and Figures 3.6 and 3.8 are the same as Figures 3.2 and 3.4, and except using ~ 4 years of MMF radar-simulated data from Aug. 1998 to Jun. 2002 with a temporal resolution of 3 hours and vertical resolution of 480 m.

3.2.1. Boundary Layer Clouds

Comparing the model annual (Fig.3.5a) and seasonal (Fig.3.7a) diurnal cycle for clouds with the observations (Figs.3.1a and 3.3a) shows that the MMF produces much smaller occurrence of boundary layer clouds than observations and there is no clear diurnal variation (Fig.3.6a and 3.8a). From Table 3.1, the daily average frequency of occurrence for boundary layer clouds in the annual composite is 2.9% for the MMF and 5.8% for the ARM ARSCL. Likewise, in summer the mean frequency of occurrence of boundary layer clouds is 1.1% for the MMF and 3.6% for ARSCL. However, this apparent lack of cloud is due in part to a known problem with the MMF, where the boundary layer clouds precipitate far too frequently [Marchand et al., 2009a], and consequently boundary layer hydrometeors have a radar reflectivity factor that exceeds our definition of cloud (dBZe < -10) most of the time. Looking at the frequency of occurrence for all hydrometeors (cloud + precipitation) (Fig.3.5d), it immediately becomes apparent that there is a diurnal variation in MMF boundary layer hydrometeors occurrence –

albeit with little evidence for any rising cloud tops in the annual or seasonal composites and with not quite the correct timing (too early). The model's boundary layer diurnal cycle is strongest in spring and to a lesser degree in autumn (which agrees with the observations), but is entirely missing during the summer.

3.2.2. High and Mid-Level Clouds

In contrast to boundary layer clouds, the MMF predicts far more high clouds than the observations in all seasons (Fig.3.7a versus Fig.3.3a). In the annual composite (Fig.3.5a), the average high cloud frequency is 15.7% (Table 3.1) and between 9.5 km and 11.5 km, the occurrence rates can reach as large as 18 - 22%, which is 8 - 12% larger than observed. Again this is a known problem with this MMF simulation [McFarlane et al., 2007; Zhang et al., 2008], and we will discuss this point later in chapter 5.

Focusing on the key features of diurnal cycle identified in observations, in spring the MMF has fewer high clouds between 3 pm and midnight, and does not capture the observed evening peak in high clouds. Rather the MMF maximum occurs in the early morning (Fig.3.7a). In summer, the model is doing better as it has a similar high cloud occurrence minimum during the day to that observed (though perhaps starting a bit sooner and ending a bit earlier) and has a broad maximum value that occurs during both evening and early morning between 10 km and 12.5 km. While, the MMF diurnal variation in high cloud occurrence is not large enough to pass the significance test (at the 95% level of confidence, Fig.3.6a and Fig.3.8a), and in spite of the excess in high clouds, it seems fair to conclude that MMF does a decent job in simulating the diurnal timing of high clouds in summer.

For mid-level clouds (Fig.3.5a and 3.7a), the (daily) mean occurrence simulated by MMF matches the observations well both in annual mean and season mean perspectives. However, the diurnal variations of the simulated middle clouds are missing or at least weaker than is observed (Fig.3.6a and Fig.3.8a).

3.2.3. Drizzle and Light Precipitation

Overall, the MMF produces much more drizzle and light precipitation than observed. Especially between 3.5 and 8 km, where the annual composite in the model (Fig.3.5b) has an occurrence rate of 6 to 12%, which is much larger than the observed 4 to 7% (Fig.3.1b). The differences are larger in winter and spring (within an absolute difference of about 4%) than in summer and autumn (about 2%) (Table 3.1). While in the observations occurrence of cloud (reflectivity < -10 dBZe) is about the same as precipitation (reflectivity > -10 dBZe) in the middle troposphere, in the MMF there is much more precipitation than clouds. Within the boundary layer drizzle and light precipitation is observed less frequently in the MMF than compared to the middle troposphere, but it still much larger than observations except in summer (when the MMF average is only 1%).

As regards the diurnal variation of light precipitation, in summer, the MMF shows a minimum in light precipitation between 9 am and 3 pm (starting slightly sooner and ending earlier than the observations) and with the mid-troposphere maximum being observed in the evening (rather than early morning). Nonetheless, the MMF appears to capture the overall observed vertical structure and its diurnal pattern in the upper and middle troposphere that is found in the observation (meaning a peak in the upper troposphere in evening which lowers in altitude over night). In the observations, an increase in early morning near-surface precipitation (light and heavy) is

associated with this structure, while in the MMF this increase in near-surface precipitation is categorized as almost entirely as heavy precipitation (rather than light precipitation). In other seasons, the MMF does not capture the observed diurnal pattern in spring or autumn (or in the annual composite), with the spring and autumn appearing to have (if anything) an unrealistic maximum in the noon and a minimum after 6 pm.

3.2.4. Heavy Precipitation

As is the case for high clouds and light precipitation, the MMF also tends to predict a larger occurrence of heavy precipitation than is observed (Fig.3.7c versus Fig.3.3c). This overestimate is seen at almost all the levels and in all the seasons except summer when the simulated heavy precipitation in the boundary is only 0.1% smaller than observations and only 0.1% larger in the upper troposphere (Table 3.1). In spring, however, the MMF predicts 2% - 3% greater occurrence of heavy precipitation below 7.5 km than is observed, which in a relative sense amounts to a three-fold increase in the occurrence of heavy precipitation.

In terms of diurnal cycle, the annual composite (Fig.3.5c) exhibits more heavy precipitation from 3 am to noon below 5 km and the occurrence gradually decreases afterwards. This makes the hours around midnight show the smallest frequency rate, which does not match the observations (which show large values overnight). Above 8 km, the diurnal pattern roughly agrees with observations, having a larger heavy precipitation occurrence during evening and early morning and relative minimum during the daytime. This diurnal variation, however, is not as strong as observed and does not pass the 95% significant test (Fig.3.6c). The poor representation of the diurnal cycle is due primarily to problems in the spring. In spring, the simulated diurnal cycle (Fig.3.7c) is very similar to that in annual composite with far too great an occurrence at all times

of day – and much larger than the summer such that it dominates the annual composite. In contrast, in summer (Fig.3.7c), the occurrence of heavy precipitation is reasonably well captured by the MMF, including with much the same vertical structure. However, near the surface (in the boundary layer), the largest occurrence rates in the MMF occur in the evening rather than in the morning. Also, above the boundary layer between 4 and 8 km, the evening peak starts at about 3 pm, both slightly earlier than the observations and slightly lower in altitude than in the observations. The MMF early morning peak above the boundary layer is lower in altitude than the evening (peak), in agreement with observations (but does not extend into the boundary layer to the degree shown in the observations as already noted above).

3.2.5. All Hydrometeors

The previous subsections show that the MMF overpredicts high clouds, as well as light and heavy precipitation, and so it is not surprising that when all hydrometeors are taken together (Fig.3.5d and Fig.3.7d) the MMF predicts a much larger total hydrometeor occurrence rate than the observations above the boundary layer (above about 2.5 km). In the observations, there is a clear diurnal cycle of hydrometeors above the boundary layer in the annual average (Fig.3.1d) that is due predominately (though not entirely) to diurnal variations in the spring and summer (Fig.3.3d) and is associated primarily with clouds and precipitation generated by deep convection and mesoscale convective systems. This diurnal variation is (at best) weakly capture in the MMF in the annual composite (and we note the small variations seen in Fig.3.5d are not significant at the 95% level of significance, Fig.3.6d). The failure of the MMF to capture the diurnal variation in the annual composite is due primarily to problems in the spring. In spring (Fig.3.7d) when hydrometeors are most plentiful, the MMF does not capture the correct diurnal timing of all hydrometeors, nor light precipitation (Fig.3.3b), nor heavy precipitation (Fig.3.3c).

In summer, on the other hand, the MMF does capture the overall vertical structure above the boundary layer for both clouds and precipitation. Nonetheless, the model evening peak starts somewhat early, (3 - 6 pm rather than 6 to 9 pm) and with more near-surface heavy precipitation in the evening rather than the morning. This suggests that while the MMF does capture MCSs during the summer to some degree, its local convection still starts somewhat earlier than it should be and likely occurs too often.

For the boundary layer, in the annual composite as well as winter, spring and autumn, the daily mean occurrence of all hydrometeors produced in the MMF is close to that shown in the observations, as quantified in Table 3.1. The diurnal cycle in spring and fall is weakly captured, though as discussed earlier, there is too much precipitation (reflectivity values > -10 dBZe) relative to cloud (reflectivity values < -10 dBZe). Also as discussed earlier, in summer, the daily mean occurrence of both clouds and light precipitation and thus all the hydrometeors are much smaller than observations and exhibits no significant diurnal variation (Fig.3.8d).

Table 3.1 Average of the hydrometeor occurrence in boundary layer (<2.5 km), middle troposphere (2.5 – 7.5 km) and upper troposphere (7.5 – 12.5 km) for cloud, drizzle and light precipitation, heavy precipitation and all hydrometeors. The corresponding values (%) in the annual (AN), winter (DJF), spring (MAM), summer (JJA) and autumn (SON) are given. For each category, the upper line is from observations and the bottom is from MMF.

Category	Boundary layer (%)					Middle troposphere (%)					Upper troposphere (%)				
	AN	DJF	MAM	JJA	SON	AN	DJF	MAM	JJA	SON	AN	DJF	MAM	JJA	SON
Clouds	5.8 2.9	6.7 3.8	7.3 3.5	3.6 1.1	5.1 2.2	4.9 4.8	6.6 6.0	5.3 5.6	3.3 3.3	4.1 3.6	7.6 15.7	7.8 17.4	8.5 18.4	8.1 13.6	5.9 12.1
Drizzle and light precipitation	3.7 4.6	4.2 8.0	4.3 4.4	2.9 1.0	3.2 3.2	4.8 7.7	5.7 9.9	5.5 9.6	4.0 4.3	3.9 5.2	1.7 4.0	0.7 2.4	2.0 5.0	3.4 6.2	1.2 3.0
Heavy precipitation	1.2 2.7	1.2 2.5	1.3 4.1	1.3 1.2	1.0 2.5	0.9 2.1	0.6 1.0	1.1 3.4	1.2 2.3	0.7 1.9	0.3 0.4	/* /*	0.3 0.7	0.7 0.8	0.1 0.4
All hydrometeors	10.7 10.2	12.1 14.4	12.9 12.0	7.8 3.3	9.3 7.9	10.6 14.7	12.8 16.9	11.9 18.6	8.5 9.9	8.6 10.7	9.6 20.1	8.5 19.8	10.8 24.1	12.1 20.5	7.2 15.5

*value is smaller than 0.1.

Table 3.2 Key Features in the Diurnal Cycle of Hydrometeors Occurrence based on Annual and Seasonal Composites for boundary layer clouds, high and middle clouds, drizzle and light precipitation and heavy precipitation for ARM MMCR observations (left) and the corresponding MMF radar-simulations (right).

Category	Key Features in the Diurnal Cycle of Hydrometeors Occurrence based on Seasonal and Annual Composites	
	ARSCL/MMCR Observations at SGP	MMF (Radar) Simulations
Boundary Layer Clouds	1. There is a significant increase in boundary layer cloud occurrence (from about 6 am to early afternoon) and cloud top lifting (from about 6 am to mid or late afternoon) in spring, summer, and autumn. 2. The diurnal variation is strongest in spring, but also easily discernable in the annual average. 3. Cloud top lifting is greater during the summer than in the spring or fall.	1. The (4 km) MMF weakly captures the diurnal increase in boundary layer cloud in the annual mean, and does so with clouds that are lightly precipitating far too frequently (and too early). The increase in cloud top is not captured in the annual or seasonal composites. 2. The diurnal variation is strongest in spring (in agreement with observations) 3. In summer, BL cloud is especially poorly captured and the model is nearly devoid of boundary layer cloud and light precipitation in summer.
High and Middle Clouds	1. In summer, high cloud occurrence shows a broad maximum extending from evening (after ~6 pm) through into early morning (~6 to 9 am), while spring has a more peaked increase with more clouds in the evening (peak near 9 pm) than in the early morning. 2. There is a very weak increase in mid level clouds in the early morning, primarily in summer but also visible in the annual composite.	1. The MMF has too much high cloud (in all seasons), but the timing of the summer variations is largely consistent with observations. In spring, the MMF high cloud occurrence peaks in early morning (rather than in the evening as found in the observations). 2. Diurnal variations of middle clouds are not present or weaker than in observations
Drizzle and Light Precipitation	1. There is a minimum occurrence of light precipitation between noon and 6 pm with a peak occurrence rate between about 4 and 8 am near the surface and in the middle troposphere. While present in all seasons (and the annual mean) this variation is strongest in summer (and is only clearly statistically significant in summer and in the annual mean). 2. In spring and summer, there is greater occurrence of precipitating particles in the upper troposphere between 8 and 12.5 km starting in the evening (6 to 7 pm) and which decreases and	1. In summer, the MMF shows a minimum in light precipitation between 9 am and 3 pm (starting sooner and ending earlier than the observations) and with the mid-troposphere maximum being observed in the evening (rather than early morning). The MMF does not capture the observed diurnal timing in spring or autumn (or in the annual composite), with the spring and autumn appearing to have (if anything) an unrealistic maximum around noon and a minimum after 6 pm. 2. To a significant degree, the MMF appears to capture the observed vertical structure and its diurnal pattern in the upper and middle troposphere in summer but NOT in spring.

	lowers in altitude into the early morning hours, and is associated with increased near-surface precipitation in the early morning hours.	The simulated near-surface precipitation associated with this structure is apparent in the heavy precipitation but not in the light precipitation category.
Heavy Precipitation	1. In the annual composite, lower troposphere (and near-surface) heavy precipitation peaks in the early morning (before 9 am) and evening (after ~ 6 pm). In the upper troposphere, large reflectivity values (heavy precipitation category) are most frequently observed in the evening (after ~ 6 pm), with a relative minimum between 6 am and 3 pm. 2. In spring, near-surface heavy precipitation is more frequent in the evening and is coincident with a peak between 4 - 7 km. 3. In summer, near-surface heavy precipitation is more frequent during the early morning. A peaks exist between about 6 - 10 km during the evening and between 5 - 7 km during early morning and tracks with a similar vertical structure in light precipitation.	1. The MMF annual composite exhibits far too much heavy precipitation in the lower troposphere with a maximum from 3 am to noon, which does not agree with observations. This is due primarily to poor representation in the spring. In the upper troposphere, there is a larger occurrence of heavy precipitation during evening and early morning, in rough agreement with the observations. 2. In spring, the MMF does not capture the observed diurnal variation, showing if anything, a slight increase between 3 am and noon. 3. In summer, the occurrence of heavy precipitation is reasonably well captured by the MMF, with much the same vertical structure. However, near the surface (in the boundary layer), the largest occurrence rates in the MMF occur in the evening rather than in the morning. Above the boundary layer, the evening peak starts at about 3 pm, both slightly earlier than the observations and slightly lower in altitude than in the observations. The MMF early morning peak above the boundary layer is lower in altitude than the evening, in agreement with observations.

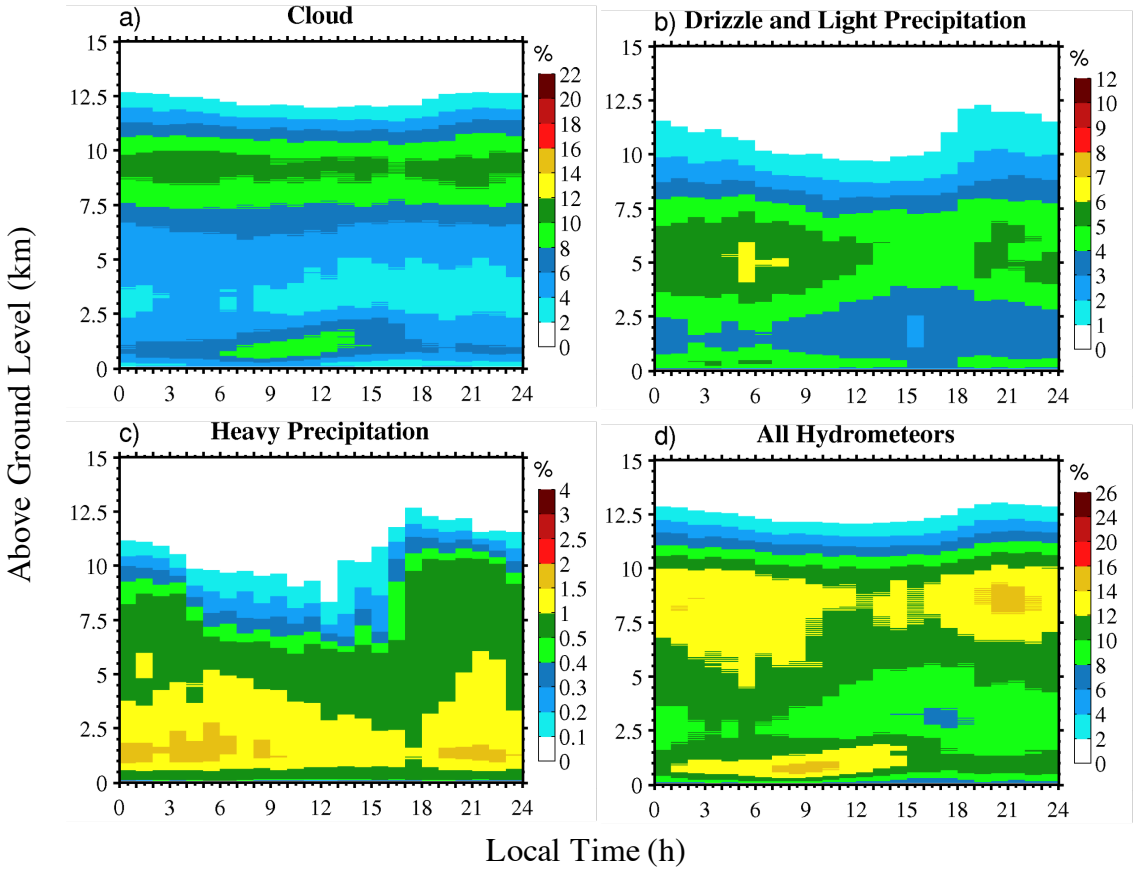

Figure 3.1 The annual diurnal cycle of clouds (a), drizzle and light precipitation (b), heavy rain (c) and all the hydrometeor occurrence (clouds + drizzle and light precipitation + heavy rain) (d) at SGP on a grid with 1 hour and 45 m grid spacing, and based on ~14 year MMCR dataset.

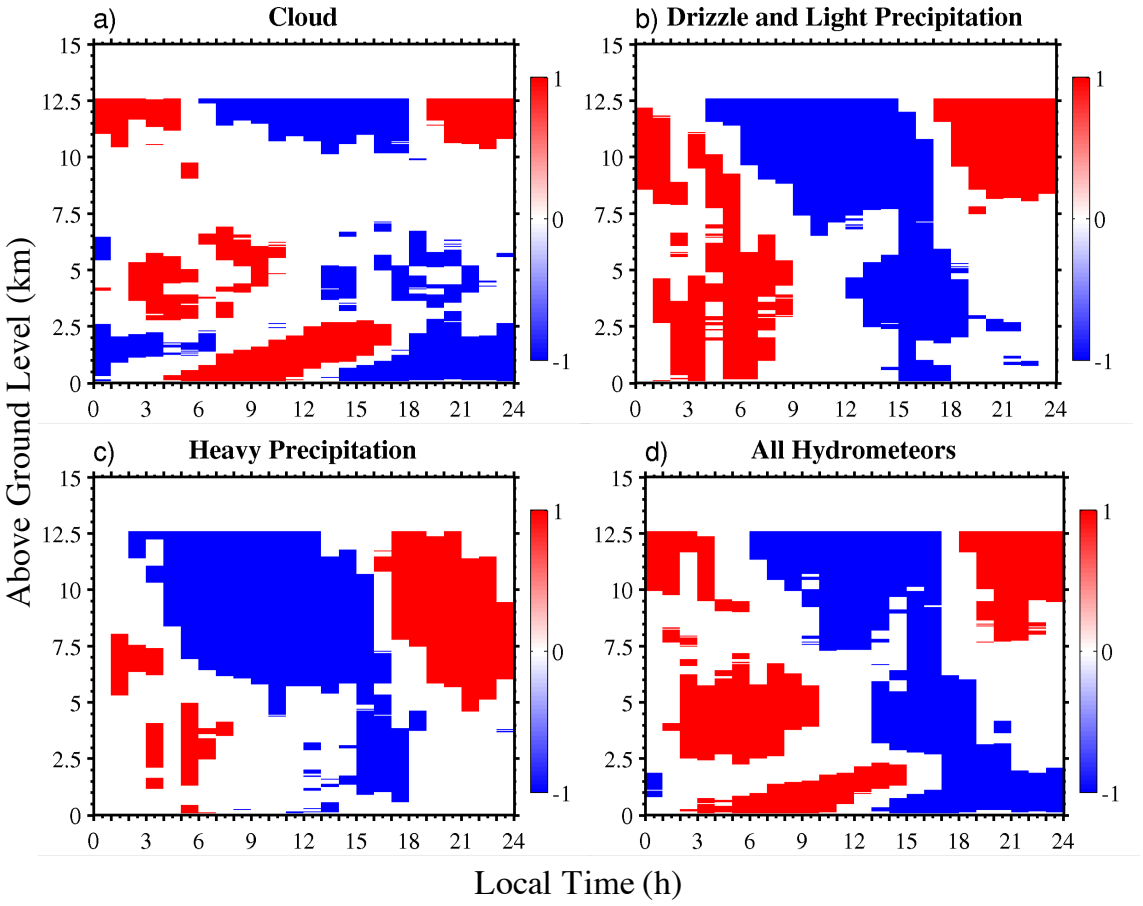

Figure 3.2 The 95% significant level using moving-bootstrap method for the corresponding annual diurnal cycle as shown in Fig. 1. Red represents that the frequency is significant larger than the rest of of the day at the same altitude. Blue represents significantly smaller and white indicates not significant. Note that when the occurrence is very small, the uncertainty of this test is very large so the results above 12.5 km are not shown.

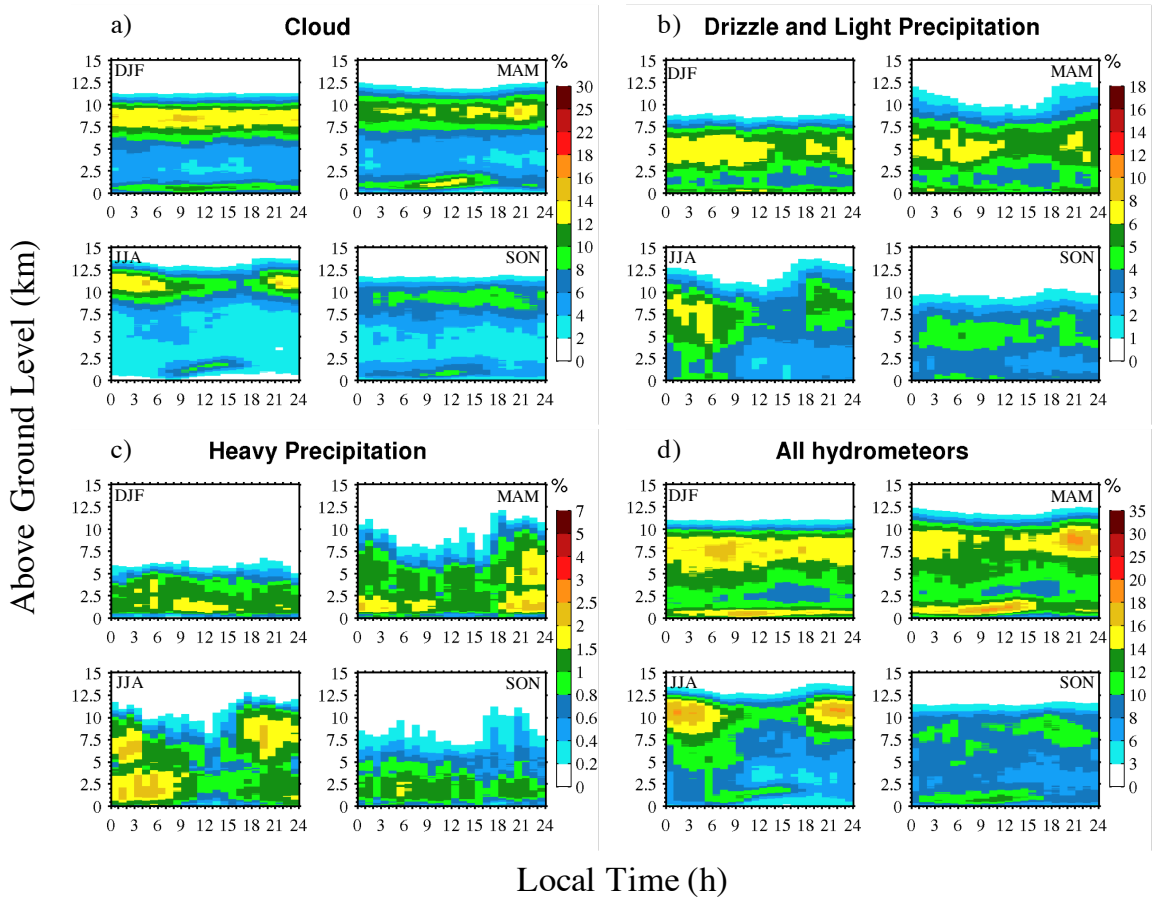

Figure 3.3 Same as Fig.3.1 except that each panel represents seasonal diurnal cycle of each category from winter (DJF) to autumn (SON).

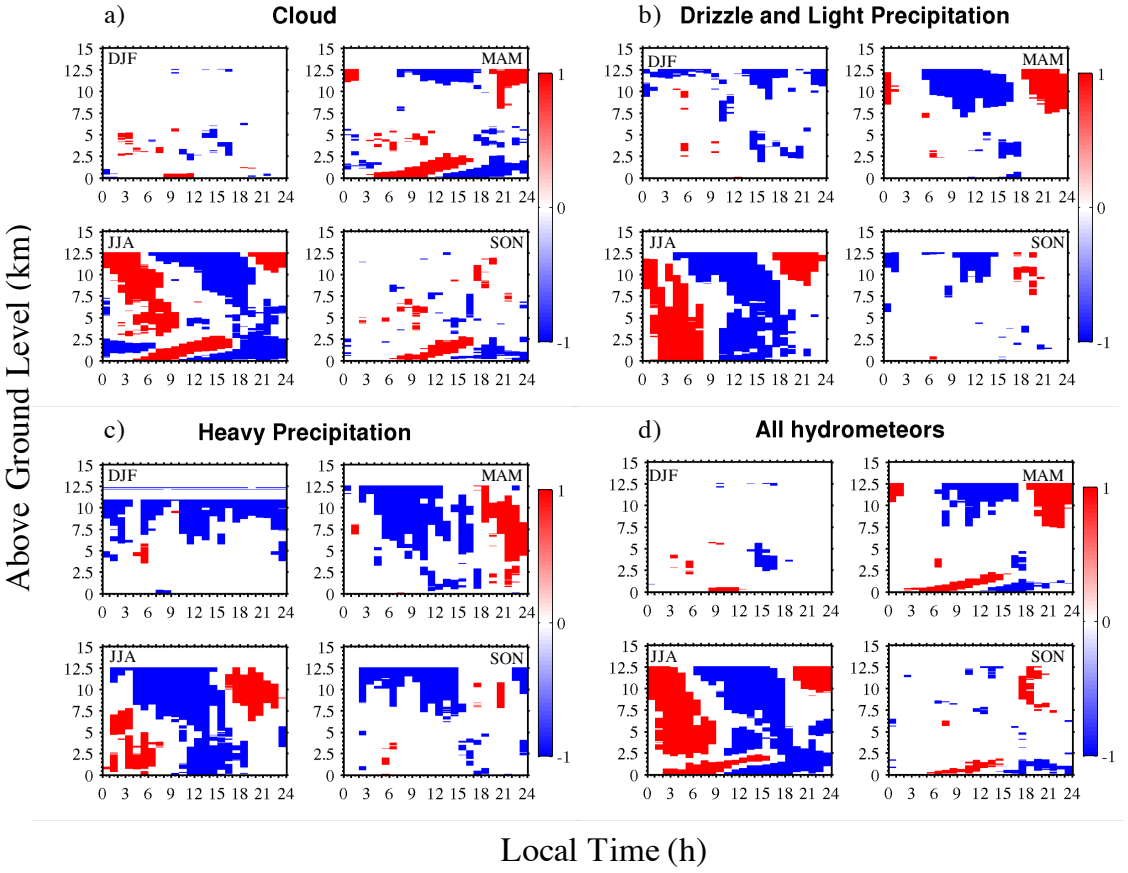

Figure 3.4 Same as Fig.3.2 except that each panel represents seasonal diurnal cycle of each category from winter (DJF) to autumn (SON).

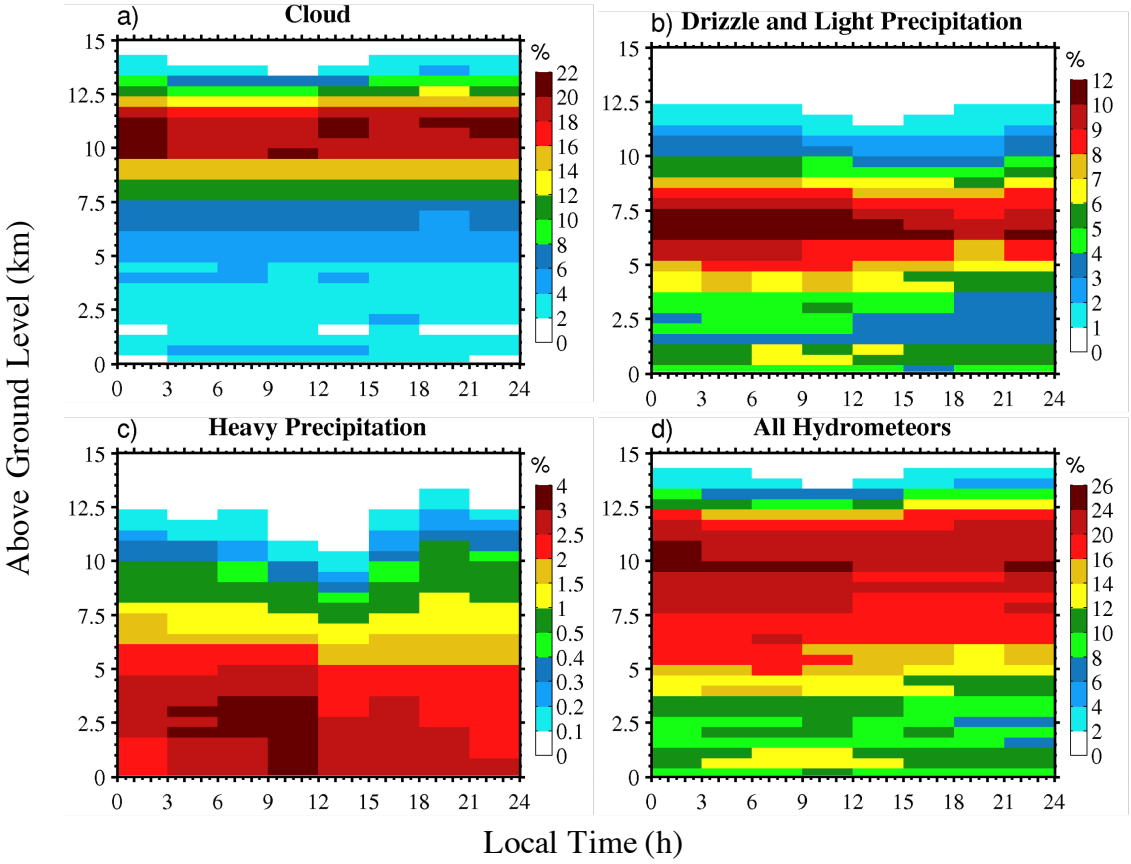

Figure 3.5 Same as Fig.3.1 except using approximately 4-year MMF-simulated data from Aug. 1998 to Jun. 2002 with a temporal resolution of 3 hours and spatial resolution of 480 m.

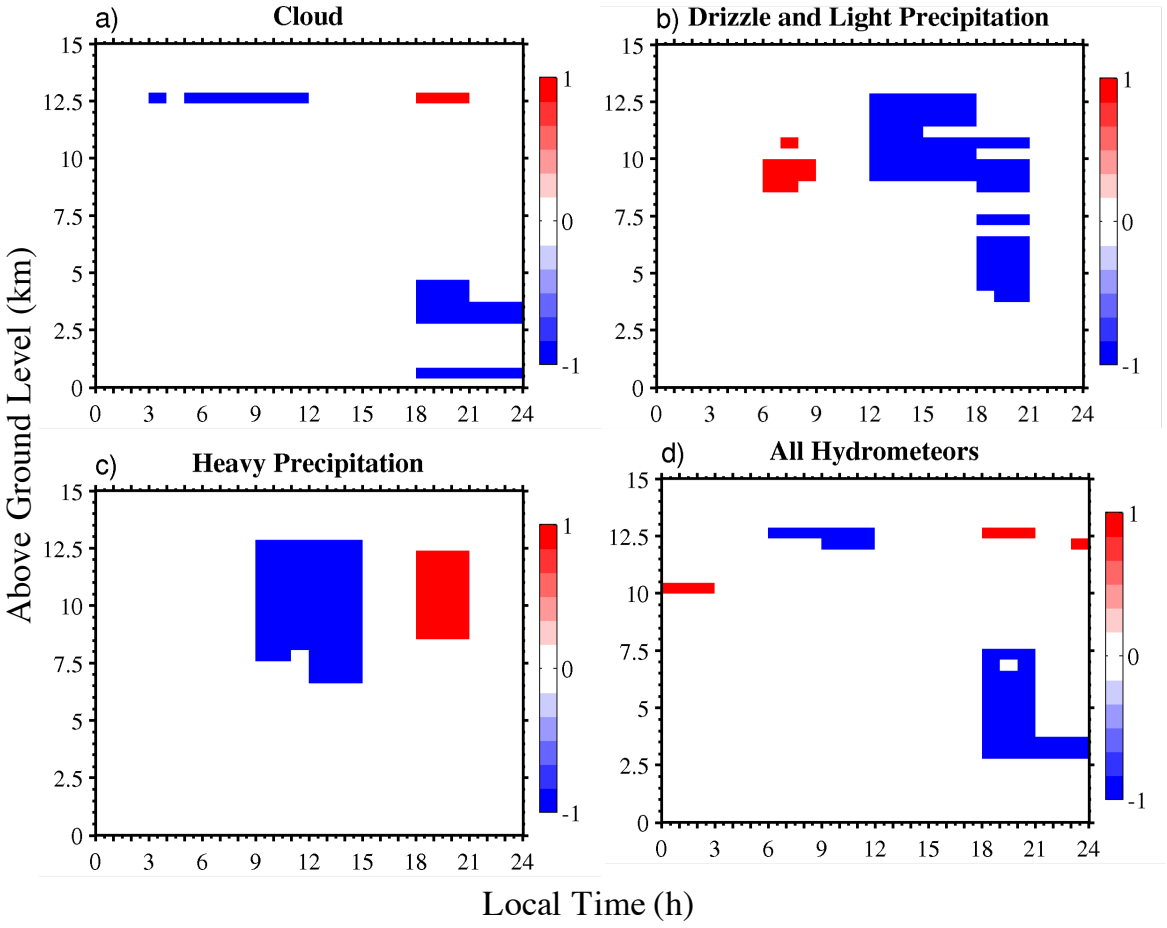

Figure 3.6 Same as Fig.3.2 except using approximately 4-year MMF-simulated data from Aug. 1998 to Jun. 2002 with a temporal resolution of 3 hours and spatial resolution of 480 m.

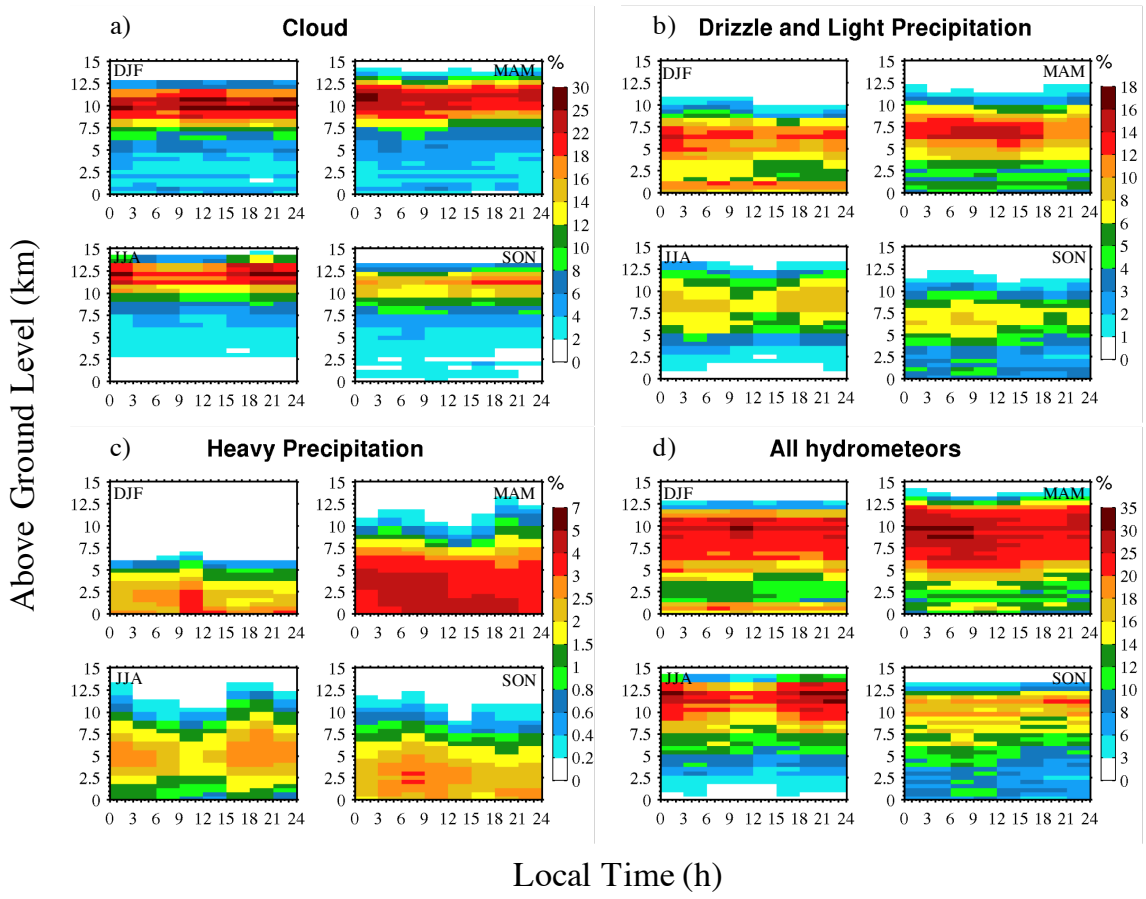

Figure 3.7 Same as Fig. 3.5 except that each panel represents seasonal diurnal cycle of each category from winter (DJF) to autumn (SON).

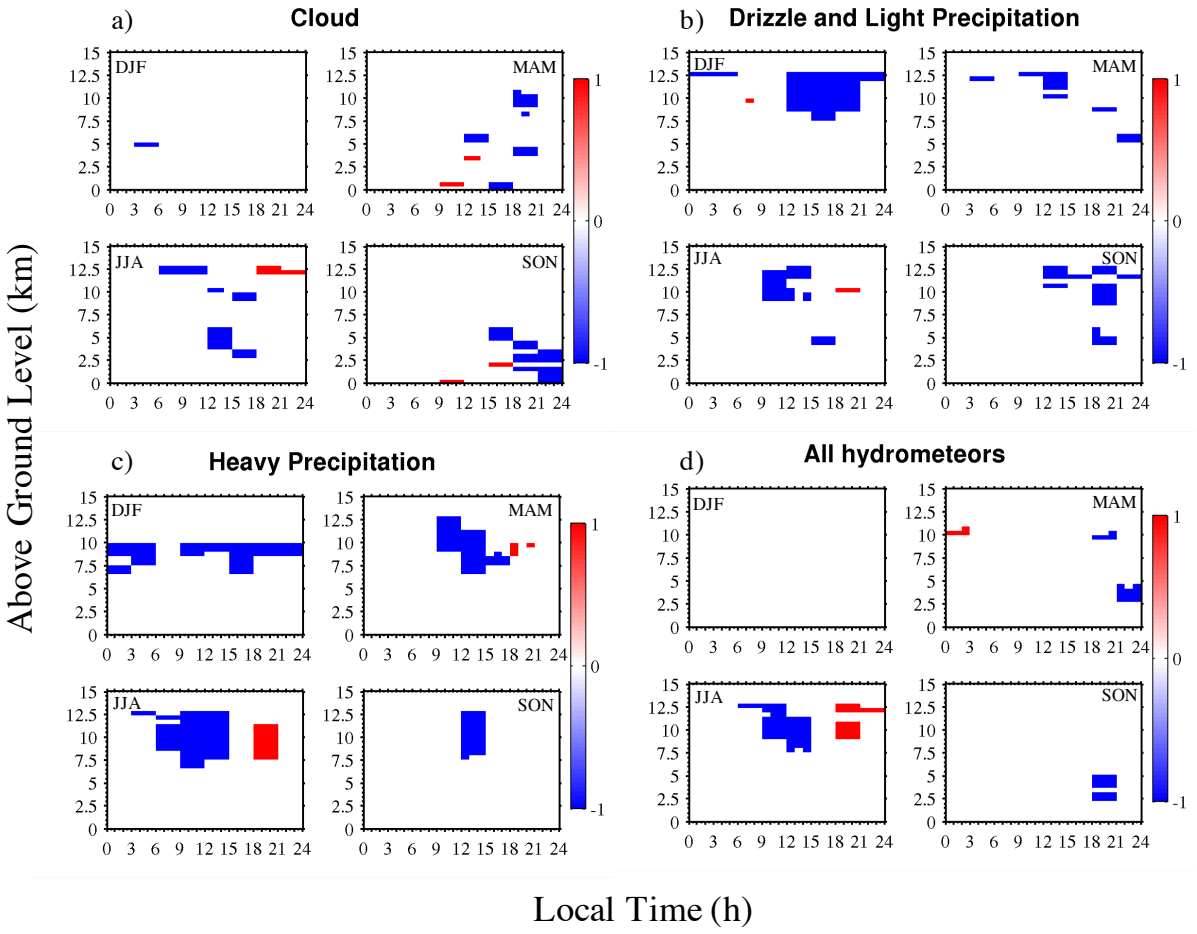

Figure 3.8 Same as Fig.3.4 except using approximately 4-year MMF-simulated data from Aug. 1998 to Jun. 2002 with a temporal resolution of 3 hours and spatial resolution of 480 m.

Chapter 4 : Atmospheric State-Based Analysis and Error Decomposition

Unlike weather forecast models, Global Climate Models (GCMs) do not generally predict the sequence of weather events that will be observed at any given site [Marchand et al., 2009b], and consequently comparisons with observations is often accomplished using annual or seasonal composites (e.g. seasonal means) as shown in chapter 3. However, the resulting differences may be due to inabilities of the model to correctly simulate the distribution of synoptic conditions or to correctly respond to a specific meteorological condition, and in some case these two error sources can cancel or conceal each other [Norris and Weaver, 2001; Evans et al., 2012].

An alternative approach is to composite data under specific dynamical regimes or various specific meteorological conditions, sometimes referred to as atmospheric states [Jakob, 2003]. Simple approaches using a single meteorological variable have been proven useful. For example, Tselioudis et al. [2000] used sea level pressure to identify low, near-normal and high pressure regimes and compared the corresponding cloud types and top of atmosphere radiative fluxes. Norris and Weaver et al. [2001] composited different observed and simulated cloud properties (i.e., cloud radiative forcing, liquid water etc.) as a function of 500 hpa pressure vertical velocity – an approach that has been widely used by other researchers [e.g. Tselioudis and Jakob 2002; Bony and Dufresne 2005]. And other parameters, such as lower tropospheric stability [Wyant et al., 2009], and surface precipitation rate [Zhang and Klein, 2010] are also frequently used to sort data when comparing composites of observational data and model outputs. Cloud regimes, clusters based on data provided by the International Satellite Cloud Climatology Project (ISCCP), has also been proven to be an effective way to classify

observations, identify model biases, and even aided in field experiment planning [Jakob and Tselioudis, 2003; Williams and Webb, 2008, Tan et al., 2013].

More sophisticated atmospheric states defined by clustering various meteorological fields at different levels have also been used [Marchand et al., 2009b; Evans et al., 2012, Kennedy et al., 2015]. Here we expand upon our earlier study in chapter 3 using the atmospheric-states that were created specifically for the ARM Southern Great Plains (SGP) site by Evans et al. [2017].

4.1. Annual diurnal cycle of clouds and precipitation

Figure 4.1 shows the annual diurnal cycle of clouds (top panels) and precipitation occurrence (bottom panels) as observed by ARM cloud radar (left panels) and simulated by the MMF (right panels). This figure is similar to that given in chapter 3, except that here the data are shown on a 3-hour (rather than hourly) grid consistent with the model output, and all reflectivity factors larger than -10 dBZe have been categorized as precipitation. Chapter 3 divided these data into light precipitation (reflectivity between -10 dBZe and 10 dBZe) and heavy precipitation (greater than 10 dBZe) categories. In regards to the present analysis we found this distinction provided little additional insight to the objectives of this chapter and so for simplicity use only a single precipitation category.

The observations show a distinct diurnal cycle of low clouds (Fig.4.1a) where cloud occurrence and cloud top are observed to increase after about 6 am and decrease in the afternoon after about 3 pm. The MMF (Fig.4.1b) simulates much smaller cloud occurrence below 2.5 km, and does not capture the observed diurnal cycle. As compared to boundary layer clouds, neither observations nor simulations show a strong diurnal cycle above 2.5 km in the annual composite. This is not true during in the summer or spring seasonal composite, or as we will see shortly, for

some atmospheric states. In general, the model cloud occurrence is somewhat small in the middle troposphere (between 2.5 and 7.5 km) but much larger in the upper atmosphere (above 7.5 km) as compared to the observations.

For precipitation, Fig.4.1c shows larger occurrence from midnight to noon below 2.5 km (5 – 6%) than the rest of the day (4 – 5%), while between 2.5 and 6.5 km above ground level, the occurrence is smallest from noon to 6 pm (5 – 6%). Above 6.5 km, reflectivity factors above -10 dBZe are less frequent, but with a clear tendency for precipitation to occur more frequently in evening and early morning and with the maximum altitude where precipitation is observed peaking around 6 pm and decreasing overnight. The occurrence of precipitation simulated by the MMF is larger than observations at all altitudes. As regards the diurnal cycle, Fig.2d shows the model has a larger occurrence from 3 am to noon below 10 km than at other times and the smallest occurrence rates occurs during evening, which differs greatly from the observations. Near the surface the model displays a shallow peak in precipitation occurrence between 6 am and noon, rather than a signature of deepening cumulus clouds as found in the observations, which is indicative of the tendency of the MMF to produce low level cloud that drizzles too frequently [Marchand et al., 2009a; Wang et al., 2015].

Using the bootstrap resampling approach, we find these diurnal variations in observations are significant at the 95% level of confidence, meaning they are not a result of sampling noise in the composite. This is not surprising given the multiyear datasets being used to construct these composites. However, once we subdivide the data into 21 atmospheric states, the sampling uncertainty becomes more noteworthy. Except where noted below, the features we discuss are (at least close to) significant with respect to sampling.

Fig.4.1, paints a rather bleak picture of the MMF diurnal cycle of cloud and precipitation, in the annual mean. Chapter 3 extended the above approach to seasonal scale, where it becomes apparent that the MMF is doing better in summer than in other seasons. Even at the season scale, however, it is not clear to what degree the observed differences between the observations and the model are due to the inability of the MMF to produce the right distribution of synoptic regimes or its inability to simulate the correct diurnal cycle under specific dynamical and thermo-dynamical conditions. To clarify the cause of the model and observational differences (which we will refer to as errors), in the following section, we composite the diurnal cycle of clouds and precipitation in terms of 21 atmospheric states representing various synoptic scale conditions.

4.2. Atmospheric State-based Diurnal Cycle and Error Decomposition

As introduced earlier, Evans et al. [2017] defined 21 atmospheric states using a neural network algorithm, and we employ these states in our analysis. Five of the states occur almost exclusively in the summer (states 17-21). The other 16 states occur in the winter, spring and fall, but with 5 states (3, 4, 8, 13, 16) occurring primarily in the spring and fall. Fig.4.2a and Fig.4.2b show the observed and MMF-simulated diurnal cycle of clouds in each state and Fig.4.3a and Fig.4.3b are counterparts of precipitation.

Fig.4.2 and Fig.4.3 demonstrates that the MMF, in a broad sense, has a reasonable cloud/precipitation response to synoptic variability. States associated with relatively small cloud/precipitation occurrence in the observations (for example #9, 10, 14, 16, 17) likewise show less cloud/precipitation in the MMF; and states with relatively large occurrence in the observations (for example #1, 2, 4, 5, 20) likewise have more simulated cloud/precipitation (especially high cloud). That said, it is also immediately clear that the model produces larger

high cloud occurrence than is observed in most states. Meanwhile, the altitude where high cloud is most frequent tends to be higher in the model as compared with the observations. For low clouds, as well, there are widespread problems. While there are some variations in the strength and timing, many of the states show an increase in the frequency of cloud below 2.5 km which begins in the morning and ends in the afternoon (specifically states # 3, 4, 6, 8, 13, 16, 18, 19, 20, 21), all of which contribute to the increase observed in the annual mean (Fig.4.1a). Few, if any, of states the model in Fig.4.2b demonstrate a clear diurnal cycle. Rather, the simulated low cloud occurrences are much smaller than observed in all of these states.

That these problems (high-cloud amount, high-cloud altitude, low-cloud amount and low-cloud diurnal variation) are manifest across many states, suggests that it is unlikely the relative occurrence of particular state (e.g. the model spends too-much or too-little time in any particular state) contributes much to the error in the annual mean. We will discuss this issue further in chapter 5.

For the remainder of the article we focus on diurnal variations in high cloud and precipitation, separated from the issue of the daily-mean intensity. The observations (Fig.4.2a and 4.3a) exhibit an obvious diurnal cycle in high clouds in state 2, 3, 16, 17, 18,19, 20, 21 and in precipitation in states 3, 6, 8,17, 18, 19, 20, 21, with (typically) a larger occurrence in the evening and/or early morning depending on the state. These states occur most frequently in summer (17, 18, 19, 20, 21), or in a few cases in spring or fall (3, 8, 16). Analysis using the bootstrap test indicates that the diurnal cycle of precipitation is likely statistically significant in all of the above states, but the change in high cloud occurrence is not significant in the spring states (2, 3 and 16) at the 95% level of confidence.

We examine the diurnal variations in states 4, 8, 19, 20, and 21 in more detail in Fig.4.4, using the decomposition introduced in chapter 2, and their synoptic conditions are shown in Fig.2.1.

The differences between observed and simulated diurnal cycle in each state can be decomposed into that caused by the daily-mean hydrometeor occurrence $\overline{(HO_i)}$ and the normalized diurnal variation $(HO_{i,t})'$ for each layer. Typically we find that $\overline{(HO_i)}$ in the model is too small in the boundary layer and too large in upper troposphere. To evaluate the contributions of these two factors, in Fig.4.4a, we show the observed diurnal cycle of cloud occurrence in the top row (same data as shown in Fig.4.2a). In the second row, we re-calculate (re-compose) the diurnal occurrence of clouds but replace $(HO_{i,t})'_{obs}$ by $(HO_{i,t})'_{mod}$. That is, the second row shows the diurnal cycle one would have in the model, if the model had same daily-mean profile as is observed. The third row in Fig.4.4a is the model diurnal cycle (same data as show in Fig.4.2b). Thus for each column (state), the differences between the second row and the first row is the difference due to normalized diurnal variation between the observations and the model; and the differences between the third row and the second row are due to daily-mean profile occurrence. Fig.4.4b shows the corresponding results for precipitation.

Comparing the low clouds in the first and second rows of Fig.4.4a, confirms (and perhaps makes more apparent) our early conclusion that the MMF does not correctly capture the diurnal variation of low cloud occurrence. If anything, the model tends to produce less low clouds at noon and more in the late afternoon or early morning, which entirely out of phase with observed low clouds. For high clouds, the observations (top row) in the summer states 19, 20 and 21, show increased high cloud in the evening or morning (depending on the state). This diurnal variation in high clouds is being captured in the MMF in the summer, although the exhibited

diurnal variations in the MMF are weaker in states 20 and 21 and stronger in state 19 than is observed. Not surprisingly, the increase in high cloud in the summer states is associated with convective precipitation. The top row of Fig.4.4b shows the observed diurnal cycle of precipitation for the same states as Fig.4.4a. We will discuss the diurnal cycle of precipitation for the summer states further, momentarily, but first we describe the less consistent behavior of the model and observations in the spring.

While the observations in both state 4 and 8 appear to show a slight increase in high clouds in the evening (perhaps more obvious in state 4), the increase is not statistically significant at the 95% level of confidence in either state. Perhaps oddly, in state 8 the observations DO show a clear diurnal cycle in regard to precipitation (Fig.4.4b), while the model in state 8, has NO clear diurnal cycle in precipitation. The situation with regard to precipitation is reversed in state 4, where the observations show NO clear diurnal cycle in precipitation, but the model DOES have a clear diurnal cycle (though it is not statistically significant). We will discuss this inconsistent behavior of the model and observations for these two spring states in more detail at the end of this chapter.

States 19, 20 and 21 all show a distinct diurnal cycle in observed precipitation. Among the five summer states, most of the total surface rain occurs in these three states, with state 20 being the wettest. Zhang and Klein [2010] classified summer precipitation at SGP into a late afternoon or early evening regime (3 to 8 pm LST) and a midnight to early morning (0 to 7 am LST) regime based on the time of the maximum surface precipitation rate. These authors generated a time series for May-August of the years 1997-2007. Most of time, the events with early morning precipitation were not locally generated [Zhang and Klein, 2010] but rather were caused by mesoscale convection systems (MCSs), which typically initiate over the Rocky Mountains and

propagate eastward [Carbone et al. 2002; Carbone and Tuttle 2008]. In Fig.4.5, we show the number of the Zhang and Klein afternoon/evening precipitation events, and the number of early morning events, for each of the five states showed in Fig.4.4 Figure 4.5 shows there are more events where precipitation peaks in the early morning in states 20 and 21, and more late afternoon or evening precipitation events in state 19. This is consistent with what we observe in Fig.4.4b, which shows a greater occurrence of precipitation in the early morning in states 20 and 21, and a greater occurrence in the afternoon in state 19. Thus we hypothesize that precipitation in states 20 and 21 is due more to MCSs, while in state 19, it is more frequently due to local (and perhaps isolated) convection.

Overall, the diurnal cycle of precipitation and high cloud occurrence for the summer states 19, 20, 21 is similar in the model to the observations. Nonetheless, looking closely we see the evening peak in precipitation occurrence appears to start somewhat early in the model (as compared with the observations) in state 20, and a bit too late and too strong in state 19. Chapter 3 showed that in the seasonal summer composite, the model tended to start earlier than the observation, but we see here this is not universal for all the summer states/conditions. The timing in the summer composite is close that that of state 20, and likely is due to the fact that state 20 is the summer states with the largest precipitation occurrence, and contribute most to the occurrence of precipitation in the summer seasonal composite.

In spring or autumn, most of the total rainfall occurs in states 4 and 8. Associated with the diurnal cycle of cloud in state 4 there is a diurnal cycle in precipitation, which is stronger in the model than in the observations. Perhaps surprisingly, the opposite is true in state 8. While there is no obvious diurnal cycle in high cloud in the observations or the model, there is a clear diurnal variation of precipitation in the observations but not in the model. State 8 typically follows in

sequence from state 4. That is, the atmospheric states we are using represent commonly occurring synoptic patterns, and naturally, these patterns represent various stages of synoptic systems and tend to fall in predictable sequence [Evans et al., 2017]

State 4, followed by state 8, captures the transition of the ARM SGP site from the warm sector of an approaching low where the front is still far from the ARM site (state 8) to the arrival and passage of a late-spring cold front (state 4) (Fig.2.1). The observations in Fig. 4.4b suggest the occurrence of precipitation near the front (state 8) is strongly modulated by the solar cycle, and this modulation is not captured in the MMF. We speculate that this may be due to the very large occurrence of high cloud that is present in the model in state 8, acting to diminish the impact of solar heating at the surface and reducing any preferred timing for convective initiation. The MMF model appears to overpredict the diurnal cycle of convection in state 4, especially in the evening. Evans et al. [2017] shows that state 4 often has CAPE values exceeding 1000 J/Kg and it is not surprising this state is observed to convectively active some of the time. This version of the MMF has been identified has having too much (or too strong) convection in previous studies [Marchand et al., 2009a], and it is not surprising that we find this occurring in late spring in state 8, as well as summer states 19 and 20, all of which feature large values of CAPE.

4.3. Error Decomposition for the annual mean diurnal cycle

Compositing the diurnal cycle state by state has enabled us to evaluate the performance of the MMF under various synoptic conditions. Using this stated-based framework we can also assess to what degree the relative frequency of occurrence of the states, the daily-mean diurnal profile, and the diurnal variations contribute to total differences. In equation (1), we can substitute in

sequence $(SF_{i,t})_{obs}$, $(HO_{i,t})'_{obs}$, and $\overline{(HO_i)_{obs}}$ by its model counterpart. The results of doing so are shown in Fig.4.6.

4.3.1. Frequency of States

The upper panels of Fig.4.6 show the results for cloud occurrence and the lower panels for precipitation. The left most panels, Fig.4.6a and 4.6f, are the observed diurnal cycle (which is the same as shown in Fig.4.1). To right of these panels we examine the impact of differences in the frequency of occurrence. Fig.4.6b and 4.6g are obtained by replacing $(SF_{i,t})_{obs}$ by $(SF_{i,t})_{mod}$ in equation (1). Comparing Fig.4.6a and 4.6b shows that differences due to the frequency of occurrence of the atmospheric states have only very small effects on low cloud and mid-level cloud occurrence but there is a slight increase in high clouds. Regarding precipitation occurrence, comparing Fig.4.6f and Fig.4.6g show the diurnal cycle of precipitation is altered. Below 2.5 km in the observations (Fig.4.6f) there is a slightly larger occurrence of precipitation in the early morning than in Fig.4.6g. Meanwhile in the middle troposphere, the minimum in occurrence shifts from noon to 6 pm (Fig.4.6f) to 3 to 9 pm (Fig.4.6g).

4.3.2. Diurnal Variations

In the next set of panels (c and h), we examine the impact of difference in the normalized diurnal variation, by substituting $(HO_{i,t})'_{obs}$ with $(HO_{i,t})'_{mod}$ in equation (1). Comparing Fig.4.6a and 4.6c shows that the model does not capture well the normalized diurnal variation of low cloud occurrence (as one might expect). Fig.4.6c shows a slight increase in high cloud occurrence in the early morning, but this increase is not significant at the 95% level of confidence.

However, comparing the diurnal variation of precipitation (comparing Figs.4.6f and 4.6h) shows the diurnal variation of precipitation in the observation is well captured by the model. In particular, Fig.4.6h shows the model captures the peak occurrence of precipitation below 7.5 km between midnight and noon, as well as the relative minimum in precipitation occurrence between noon and 6 pm. Perhaps the most noteworthy shortcoming in the model is an underestimate in magnitude of the evening increase (just after 6 pm) and a lower maximum altitude for precipitation at this same time (note the observations show a precipitation occurrence of 1 to 2 % extending to up 12.5 km, and the model is a bit lower). Thus as regards to overall diurnal cycle of precipitation, we conclude that the error in the annual composite is largely due to the frequency of occurrence of the states, more than the ability of the model to represent the diurnal cycle correctly in individual states. This is not to say the model respond correctly to the large scale forcing in every state (see discussion in section 4.2) but rather that error in the diurnal variations in the individual states combine to produce little errors in the annual composite.

4.3.3. Daily-mean Profile

In panels d and i, $\overline{(HO_i)_{obs}}$ is replaced by $\overline{(HO_i)_{mod}}$ in equation (1), which shows the impact of difference in the daily-mean profile. As is immediately evident from the appearance of red colors in these two panels, most of the error in the model cloud and precipitation occurrence is present in the daily-mean profile. As noted in the beginning of this chapter, the model has (1) too much high cloud that is too high in altitude, (2) too high an occurrence of precipitation at all altitudes, and (3) too little low cloud. For completeness, the last set of panels e and j, show the full model results (that is, the result of equation 2, or equivalently, where all three terms in equation (1) have been swapped). Comparing Fig.4.6i and 4.6j again highlights the shift in

precipitation timing which is due primarily to the frequency of states rather than errors in individual states.

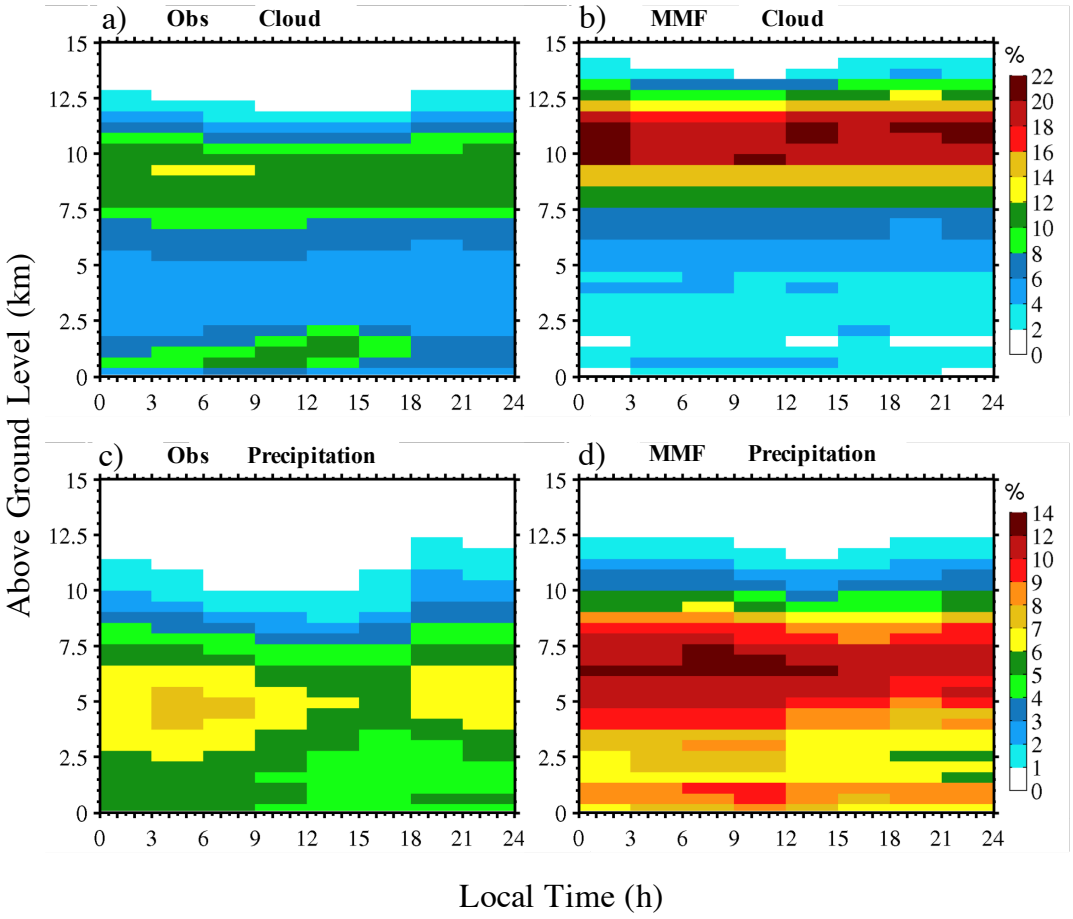

Figure 4.1 The observed annual diurnal cycle of clouds (a) and precipitation (c) and the corresponding model simulations (c and d, respectively) at SGP with 3 hour and 480 m resolution. Time is local time (UTC - 6).

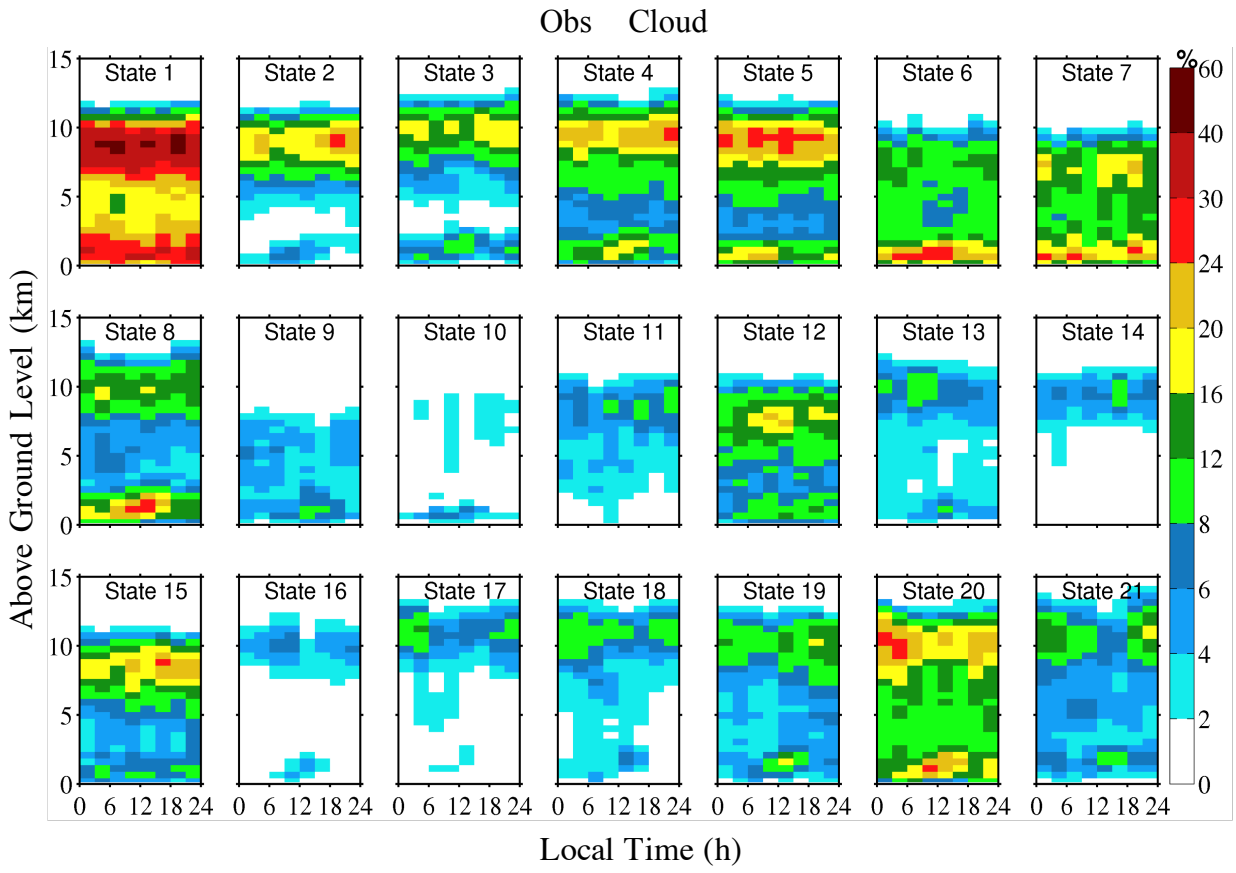

Figure 4.2a The observed annual diurnal cycle of clouds for all the atmospheric states

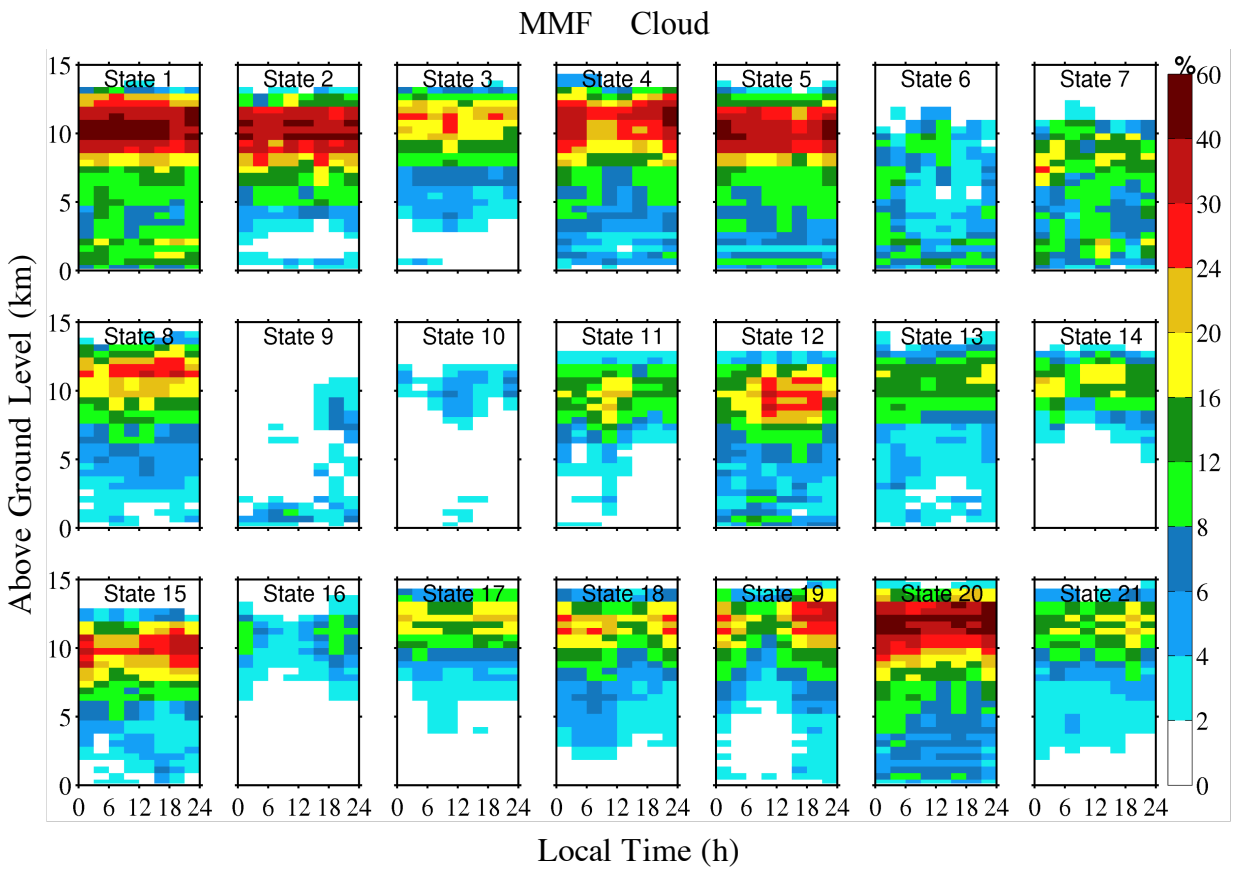

Figure 4.2b. The simulated diurnal cycle of clouds for all the atmospheric states

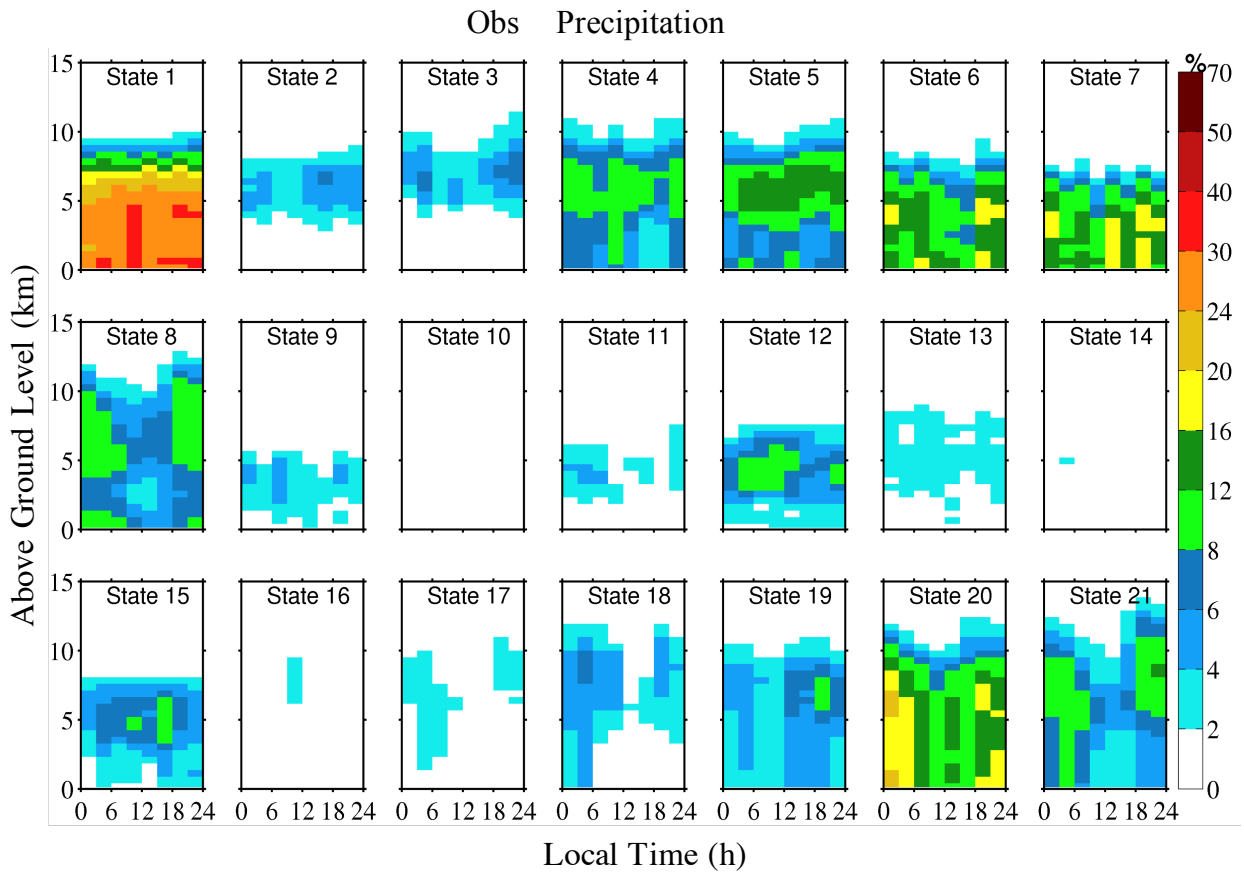

Figure 4.3a The observed diurnal cycle of precipitation for all the atmospheric states.

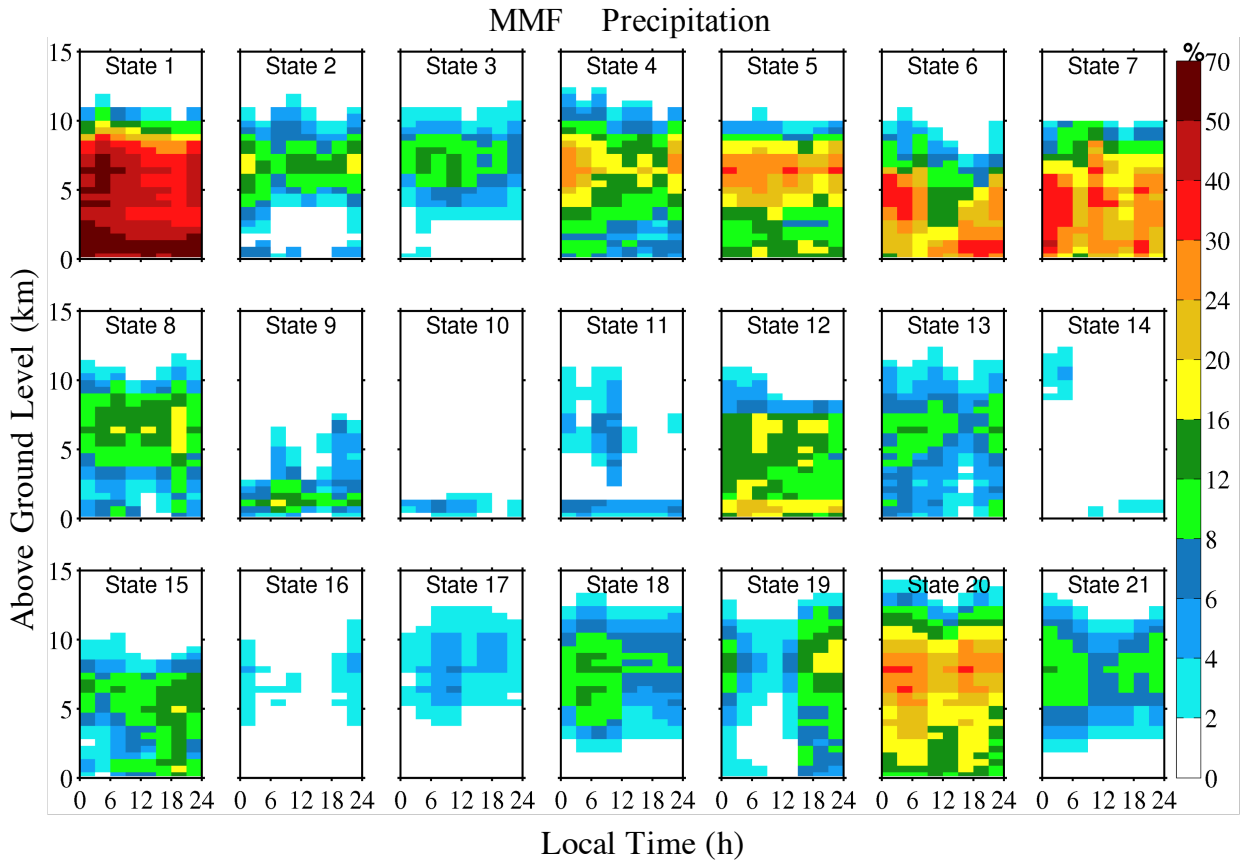

Figure 4.3b The simulated diurnal cycle of precipitation for all the atmospheric states

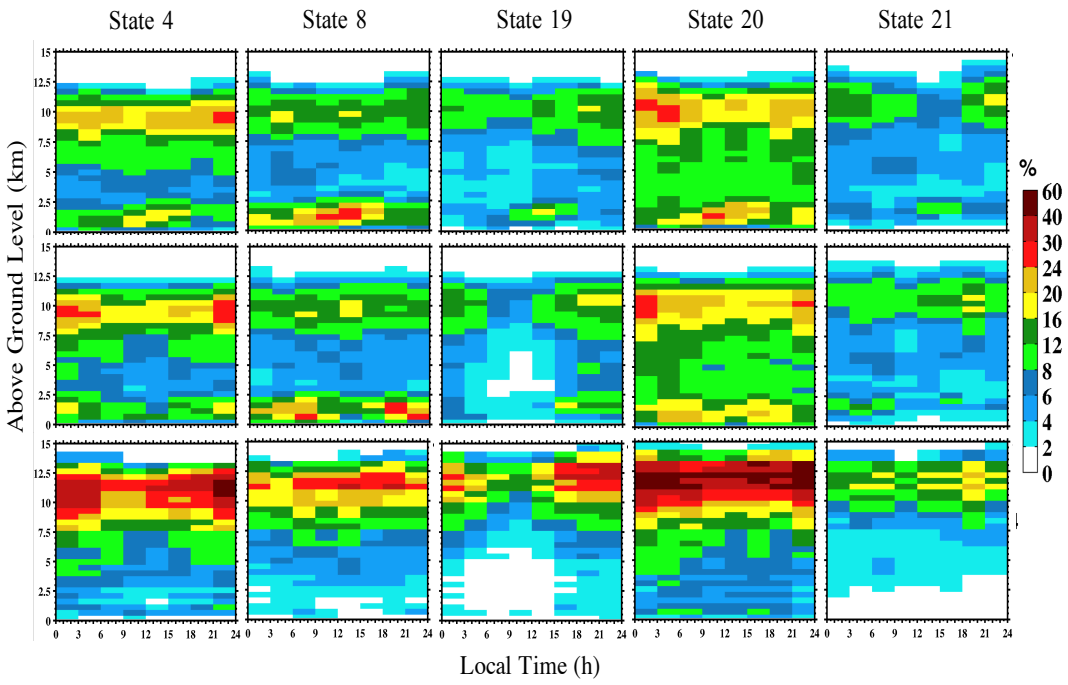

Figure 4.4a Comparison of observed and MMF diurnal cycle for select states. Top row shows the observed diurnal cycle of clouds for state 4, 8, 19, 20 and 21 and the bottom row is the corresponding plot for the MMF; Middle row is the same as top row with $(\mathrm{HO}_{i,t})'_{obs}$ replaced by $(\mathrm{HO}_{i,t})'_{mod}$, such that middle row shows what the model diurnal cycle would look like if the daily-mean (intensity) in the model was correct but the model diurnal variation was unchanged.

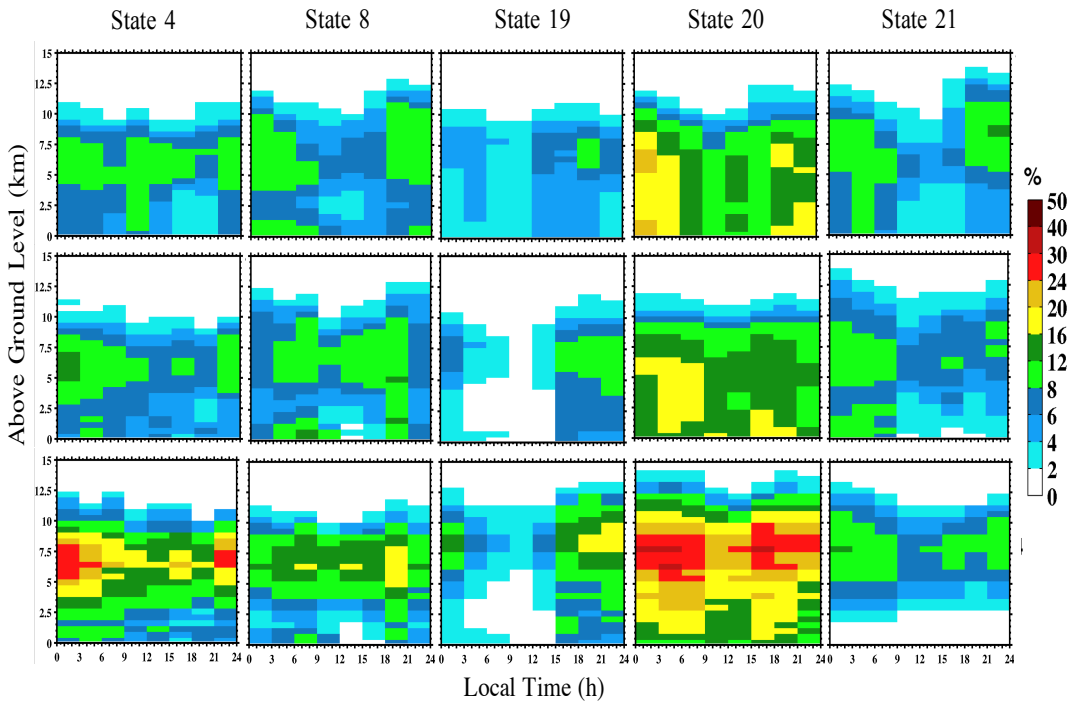

Figure. 4.4b. Same as Fig.5a but for precipitation

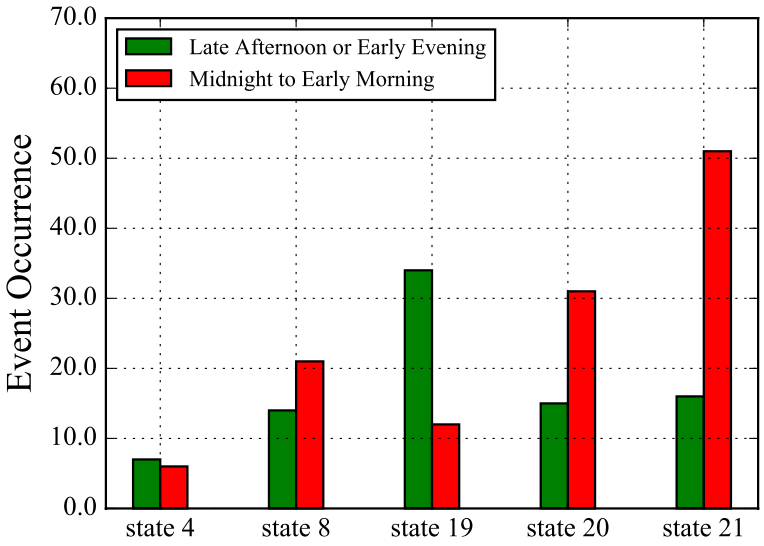

Figure 4.5 Distribution of number of state occurrence with late afternoon or early evening deep convection (green) and with midnight to early morning deep convection (red). The classification of late afternoon or early evening and midnight to early morning deep convection was done by Zhang and Klevin (2010).

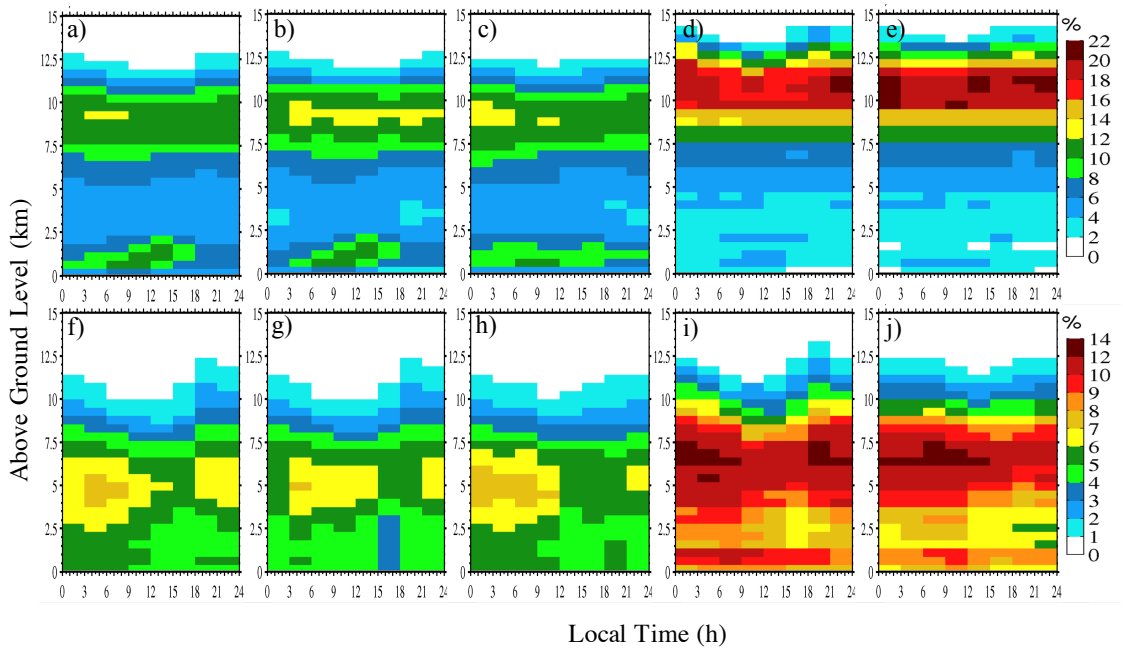

Figure 4.6 Panels a, e, f, and j are the same as Fig.1a, b, c, d, respectively. They are put here for direct comparison. Panels b and g are annual diurnal cycle of clouds and precipitation after changing $(SF_{i,t})_{obs}$ to $(SF_{i,t})_{mod}$, respectively. Panels c and h are obtained by changing $(HO_{i,t})'_{obs}$ to $(HO_{i,t})'_{mod}$. Panels d and i are obtained by replacing $\overline{(HO_i)_{obs}}$ by $\overline{(HO_i)_{mod}}$.

Chapter 5 : Conclusions and Discussions

Taking advantage of the high temporal and vertical resolution of the DOE ARM program vertically pointing MMCR and using a radar simulator with the MMF climate model, we created annual and seasonal composites of the diurnal cycle of hydrometeor occurrence for the ARM SGP site from both observations and model simulations. We classified the hydrometeors into cloud (-40 dBZe ≤ reflectivity < -10dBZe), drizzle and light precipitation (-10 dBZe ≤ reflectivity < 10dBZe), and heavy precipitation (reflectivity ≥ 10dBZe) categories. Our objectives were to (1) identify what diurnal variations are evident in annual and seasonal composites of the MMCR reflectivity profile measurements, (2) evaluate the degree to which a cloud radar-simulator in combination with the reflectivity categories might be useful in evaluating climate models, and potentially other models, (3) further evaluate the performance of the MMF model in the annual and seasonal composite and (4) in different atmospheric states. The MMF model has been shown to capture the diurnal cycle of surface precipitation better than most models [Khairoutdinov et al., 2005, 2008, Pritchard and Sommervile, 2009a], and to be able to capture the diurnal cycle of high clouds over tropical land [Zhang et al., 2008] and have MCS-like propagation patterns [Pritchard et al., 2011].

We find that, in spite of the fact that the ARM radar is vertically pointing (rather than scanning), its data record is long enough to capture important aspects of the diurnal cycle of hydrometeors and provide insight into the diurnal variations of hydrometeor vertical structure. The left column of Table 3.2 summarizes features of the diurnal cycle that were observed in the ARM radar data. A bootstrap resampling technique was used to ensure that these diurnal features represent real variations and are not a result of uncertainty in sampling. The simple classification approach

based upon different reflectivity thresholds, while it certainly does not unambiguously separate cloud from precipitating hydrometeors, was clearly useful in helping to isolate variations in precipitation that are easily missed when compositing all radar detections (because the frequency of cloud is typically much larger than the occurrence of precipitating hydrometeors).

The results of this study also demonstrate that a radar simulator combined with the simple reflectivity-based classification can be an effective approach for evaluating diurnal variations in model hydrometeor occurrence. The radar simulator nominally ensures that effects related to the instrument sensitivity and signal attenuation are taken into consideration in the comparison. Of course, that does not mean the radar simulator approach is free from uncertainties or ambiguities [e.g., see discussion Di Michele et al., 2012]. The simulated radar reflectivity is dependent on the model microphysical representation and assumptions. So, for example, the conclusion that the MMF produces too much high cloud (or at least the degree to which this is true) depends on the size (distribution) and density of the model's condensed ice. The MMF could be modified to produce (or assume) smaller and/or denser ice crystals and thereby lower the simulated radar reflectivity. But doing so will impact the fall velocity and sedimentation of ice, which is a factor that is well known to have a large impact on the amount of high cloud produced by models and to have a large impact on climate simulations. In our view, one should not use one-set of microphysical assumptions for the radar simulator and another-set for other aspects of the model physics – rather the model should have a single self-consistent representation (or set of assumptions) regarding the microphysics. In effect, the radar-simulator-based comparison is evaluating the model in total, including the validity of the microphysical representation. So in a sense, the radar simulator approach is more ambiguous. We do not know if our conclusion that the MMF produces too much high cloud may (to some degree) be due to the microphysical

representation having particles that are too large (on average) or the wrong density, or simply too large a volume filled with ice condensate. An analysis of the model results against in situ or remote sensing retrievals will be needed to further understand the role of microphysics [e.g., Yuan et al., 2006]. As such, a radar-simulator-based analysis does not replace nor reduce the importance of microphysical retrievals or in situ measurements; it is simply a tool to help evaluate the model in total, avoid sampling biases (e.g. because microphysical retrievals often work well only on certain cloud types), and help identify where (or when) problems exists and point to situations where a more in depth analysis is needed.

The atmospheric state analysis shows that the MMF responds reasonably to the large scale forcing, meaning the MMF simulates smaller cloud and precipitation occurrence in dry states compared to moist states, in a similar manner to the observations. However, the MMF model does not capture well the diurnal cycle of boundary layer clouds in all situations (the annual and seasonal composite as well as each state). Previous evaluations of the MMF have shown that this model underestimates boundary layer cloud occurrence [e.g. Marchand and Ackerman, 2010; Cheng and Xu, 2013] and this appears to be especially acute over the SGP. This is a common problem for GCMs [Klein et al., 2013]. As regards the MMF in particular, the coarse 4 km horizontal resolution and small number of vertical layers (26 total with 6 in the boundary layer) used in these simulations make it difficult to represent boundary layer thermodynamical structure, subgrid turbulence and cloud microphysical processes. Wang et al. [2015] among others have pointed toward the MMF having an overly effective auto-conversion leading to excess drizzle which likely impacts the diurnal variations of both clouds and drizzle in the boundary. Accurate simulation of the advection of atmospheric humidity is also vital to the formation of boundary layer clouds and the diurnal cycle [Khairoutdinov et al., 2008; Zhang and

Klein, 2010]. Figure 5.1 shows the diurnal cycle of relative humidity for various seasons from (a) ECMWF interim reanalysis data and (b) the MMF model. The MMF significantly underestimates relative humidity in the boundary layer in each season, and this is particularly severe during the summer (when surface temperatures are also too high in the MMF). The reasons for this are not obvious. The SGP often features a low level jet at night which advects moisture from the Gulf of Mexico over the ARM SGP site. The MMF appears to produce a strong low level jet at the right time, but with insufficient moisture (Figure 5.2). We also find that the sensible heat flux in the MMF is too large while latent heat flux is too small around noon and early afternoon as compared with Energy Balance Bowen Ratio system (EBBR) measurements at SGP (Figure 5.3 and 5.4). These surface flux errors indicate a lack of moisture in the soil or the weak transpiration from canopy in the model, which was also found by Demott et al. [2007] for the MMF.

The overprediction of high cloud and excessive upper level humidity (as we also find here) has been recognized in other MMF studies [McFarlane et al., 2007; Zhang et al., 2008]. It has been suggested that this is related to the overestimation of vertical transport of humidity [Zhang et al., 2008], the adoption of periodic lateral boundary conditions in the cloud resolved model embedded in MMF [Luo et al., 2006; Liu et al., 2015], and problems with the parameterization of the ice cloud microphysics [Khairoutdinov et al., 2008].

In regards to the present analysis, in particular, we find that the much of the difference in the annual mean diurnal cycle of high clouds and precipitation occurrence is largely due to daily-mean vertical profile differences, the frequency of occurrence of the states, rather than the ability of the model to represent the diurnal variation correctly in individual states. However, it does not necessary mean that the diurnal variation in the model is good in every season or state. In

summer, the diurnal cycle of high clouds, as well as light and heavy precipitation in the upper troposphere are reasonably well-represented in the MMF. In particular, diurnal variation in vertical structure suggests the MMF is capturing MCS propagation during the summer, supporting the conclusion by Pritchard et al. [2011]. Nonetheless, the occurrence of these hydrometeors begin to increase a bit early 3 to 6 pm instead of 6 to 9 pm suggesting that deep convection (at least some of the time) tends to occur slightly earlier than it should. This phenomenon is not universal for all the summer states. In conditions where convective precipitation peaks during the afternoon or evening (state 19) the precipitation appears to start a bit late, while in conditions where precipitation peaks during the early morning hours (states 20 and 21) - likely due to mesoscale convective systems - precipitation appears to start somewhat earlier in the day.

A surprising finding is that in spring, diurnal variations in the MMF simulated occurrence of high clouds, as well as precipitation, are not in phase with observations or even out of phase as indicated by state 4 and 8. It is not immediately clear why the MMF is doing well in representing the diurnal cycle of deep convection and MCSs in the summer and not the spring. It appears that while the MMF is able capture deep convection (and MCSs) when strongly forced, it fails to do so in the spring when surface heating is weaker. In particular, we see that it is with-in atmospheric state #8, which occurs primarily in the spring, where the observations show a strong diurnal cycle of precipitation but the model has no diurnal signature. One possible reason is that this model is able to react properly in the strong forced summer environment, but in spring or autumn states, the model excessive high clouds could further reduce the weaker surface heating and inhibit convection in the MMF from initiating at the right time. We are currently investigating this situation in more depth.

It will require detailed and careful analysis, to untangle the degree to which each of these factors contribute to the low and high clouds problem. For example, simulations where the surface moisture in the model is forced to match observations might provide insight on the degree to which soil-moisture (or the local land-surface model) rather than other factors dominate. Or simulations where the MMF resolution and vertical layers are increased (at least local to the SGP) might be used to probe this factor. Regardless, the situation is complex where errors that cause the surface becoming too dry (e.g. poor advection of water vapor) likely result in a reduction of boundary layer clouds that further surface drying. That is, there are likely positive feedbacks, which may not be entirely local. While the state-based analysis approach used in chapter 4 has a variety of weaknesses, it does provide a path to evaluate climate model errors in a "free running" climate model, meaning model simulation where the large-scale forcing is not prescribed (as is typically needed when doing case study analysis) and where feedbacks between large-scale circulation and small-scale processes can fully evolve.

In any case, we conclude by noting that datasets need to run model simulations (including case studies) and evaluate models output are being produced by the DOE ARM program; and in particular, the analysis presented in this thesis demonstrates that the ARM radar data capture diurnal variations of hydrometeor vertical structure and can be (and should be) used as part of future model development and evaluation activities.

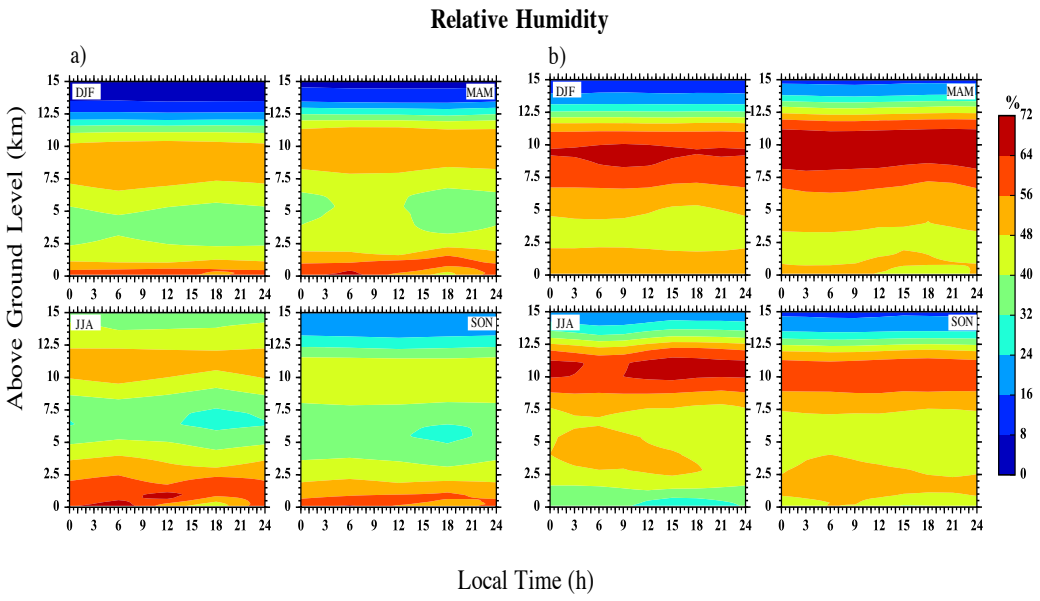

Figure 5.1 Diurnal cycle of relative humidity in four seasons from the ECMWF interim reanalysis data (left) and that from the MMF simulations (right).

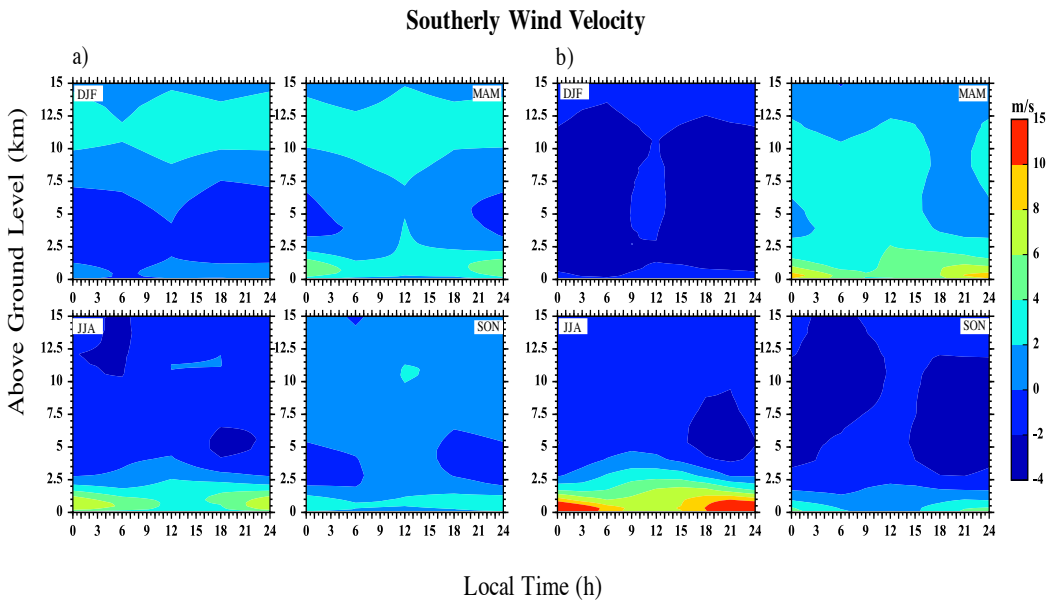

Figure 5.2 Diurnal cycle of southerly wind velocity in four seasons from the ECMWF interim reanalysis data (left) and that from the MMF simulations (right).

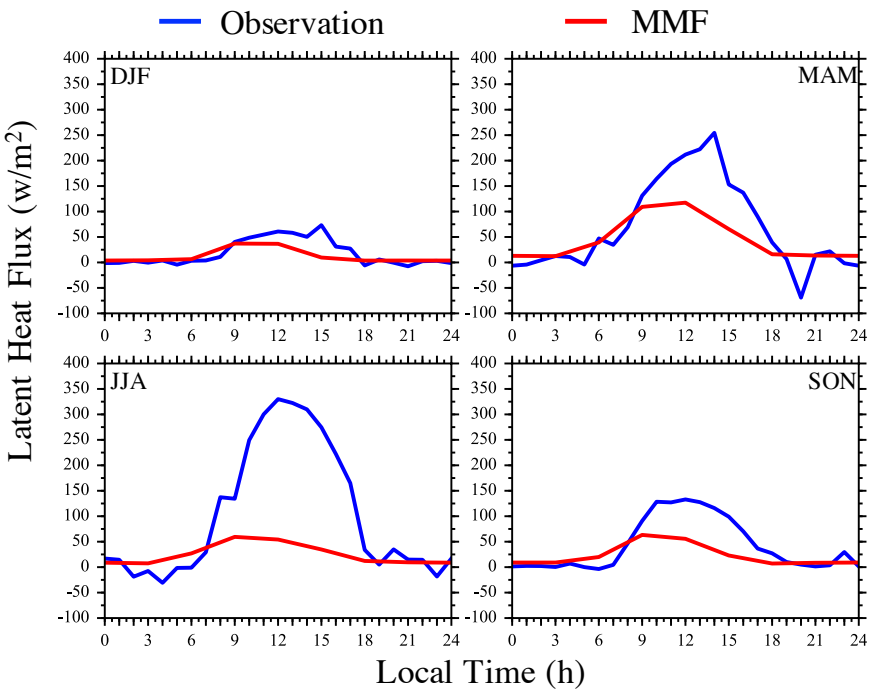

Figure 5.3 Diurnal cycle of latent heat flux in four seasons from Energy Balance Bowen Ratio (EBBR) system (blue line) at ARM SGP site and from the MMF simulations (red line). Positive value represents energy is lost from the surface.

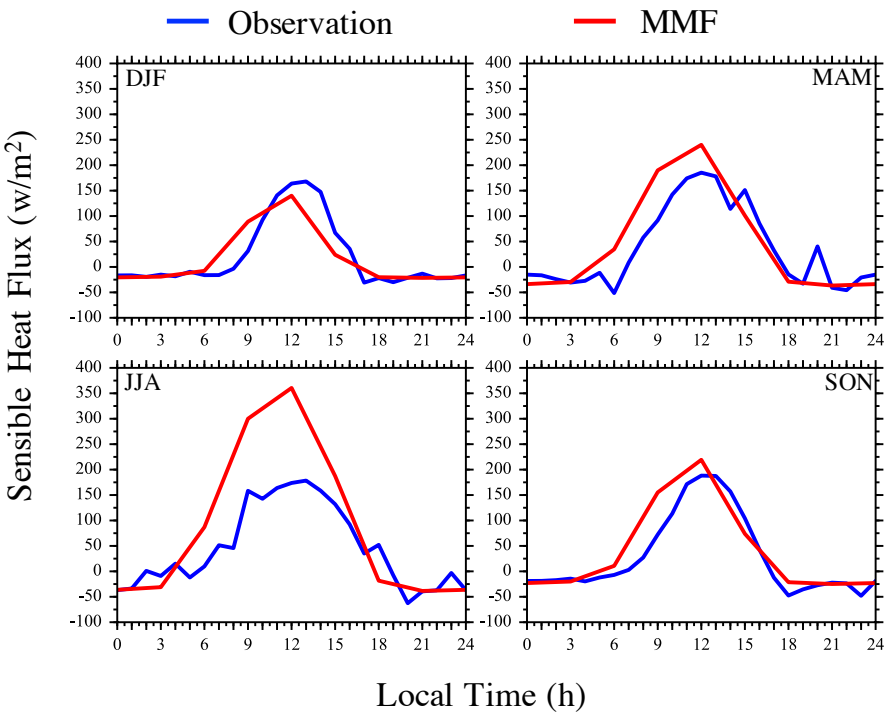

Figure 5.4 Same as Fig. 5.3 except for sensible heat flux.

Bibliography

Angevine, W. M., H. K. Baltink, and F. C. Bosveld (2001), Observations of the morning transitions of the convective boundary layer, *Boundary Layer Meteorol.*, **101**, 209–227.

Bergman, J. W., and M. L. Salby (1997), The role of cloud diurnal variations in the time-mean energy budget, *J. Clim.*, **10**, 1114–1124.

Bodas-Salcedo, A., et al. (2011), COSP: Satellite simulation software for model assessment, *Bull. Amer. Meteor. Soc.*, **92**, 1023–1043.

Bony, S., and J.-L. Dufresne (2005), Marine boundary layer clouds at the heart of tropical cloud feedback uncertainties in climate models, Geophys. Res. Lett., 32, L20806, doi:10.1029/2005GL023851.

Carbone, R. E., J. D. Tuttle, D. Ahijevych, and S. B. Trier (2002), Inferences of predictability associated with warm season precipitation episodes, *J. Atmos. Sci.*, **59**, 2033–2056.

Carbone, R. E., and J. D. Tuttle (2008), Rainfall occurrence in the U.S. warm season: The diurnal cycle, *J. Clim.*, **21**, 4132–4146.

Cheng, A., and K.-M. Xu (2013), Evaluating low cloud simulation from an upgraded multiscale modeling framework, Part III: Tropical and subtropical cloud transitions over the northern Pacific, *J. Clim.*, **26**, 5761–5781, doi:10.1175/JCLI-D-12-00650.1.

Clothiaux, E. E., T. P. Ackerman, G. G. Mace, K. P. Moran, R. T. Marchand, M. A. Miller, and B. E. Martner (2000), Objective determination of cloud heights and radar reflectivities using

a combination of active remote sensors at the ARM CART sites, *J. Appl. Meteorol.*, **39**, 645–665.

Collier, J. C., and K. P. Bowman (2004), Diurnal cycle of tropical precipitation in a general circulation model, *J. Geophys. Res*., **109**, D17105, doi:10.1029/2004JD004818.

Collins, W. D., et al. (2006), The formulation and atmospheric simulation of the Community Atmosphere Model: CAM3, *J. Clim.*, **19**, 2122–2161.

Covey, C., P. Gleckler, C. Doutriaux, D. Williams, A. Dai, J. Fasullo, K. Trenberth, and A. Berg (2016), Metrics for the Diurnal Cycle of Precipitation: Toward Routine Benchmarks for Climate Models. *J. Clim.,* **29**, 4461–4471, doi: 10.1175/JCLI-D-15-0664.1.

Dai, A., F. Giorgi, and K. Trenberth (1999), Observed and model-simulated diurnal cycles of precipitation over the contiguous United States. *J. Geophys. Res.*, **104**(D6).

Dai, A., and K. E. Trenberth (2004), The diurnal cycle and its depiction in the Community Climate System Model, *J. Clim.*, **17**, 930–951.

Dai, A. (2006), Precipitation characteristics in eighteen coupled climate models, *J. Clim.*, **19**, 4605–4630, doi:10.1175/JCLI3884.1.

Dee, D. P., et al. (2011), The ERA-Interim reanalysis: configuration and performance of the data assimilation system, *Quart. J. Roy. Meteor. Soc.*, **137**, 553–597.

Demott, C. A., D. A. Randall, and M. Khairoutdinov (2007), Convective precipitation variability as a tool for general circulation model analysis, *J. Clim.*, **20**, 91–112.

Di Michele, S., et al. (2012), Interpretating an evaluation of the ECMWF global model with CloudSat observations: Ambiguities due to radar reflectivity forward operator uncertainties, *Q. J. R. Meteorol. Soc.*, **138**, 2047–2065, doi:10.1002/qj.1936.

Dong, X., B. Xi, and P. Minnis (2006), A climatology of midlatitude continental clouds from the ARM SGP Central Facility. Part II: Cloud fraction and surface radiative forcing. *J. Clim.*, **19**, 1765–1783.

Easterling, D. R., P. J. Robinson (1985), The diurnal variation of thunderstorm activity in the United States, *J. Clim. Appl. Meteorol.*, **24**, 1048–1058.

Evans, S. M., R. T. Marchand, T. P. Ackerman, and N. Beagley (2012), Identification and analysis of atmospheric states and associated cloud properties for Darwin, Australia, J. Geophys. Res., 117, D06204, doi:10.1029/2011JD017010.

Evans, S. (2014), Atmospheric classification as a cloud and precipitation evaluation tool in models and observations, Ph.D thesis.

Evans, S., (2017), Diagnosing cloud biases in the GFDL AM3 model with atmospheric classification, J. Geophys. Res., under review.

Fritsch, J. M., R. J. Kane, C. R. Chelius (1986), The contribution of mesoscale convective weather systems to the warm-season precipitation in the U.S., *J. Clim. Appl. Meteorol.*, **25**, 1333–1345.

Frisch, A. S., C. W. Fairall, and J. B. Snider (1995), Measurement of stratus cloud and drizzle parameters in ASTEX with a Ka-band Doppler radar and a microwave radiometer, J. Atmos.

Sci., 52, 2788–2799.

Houze, R. A. (2004), Mesoscale convective systems, *Rev. Geophys.*, **42**, RG4003, doi:10.1029/2004RG000150.

Haynes, J., R. T. Marchand, Z. Luo, A. Bodas-Salcedo, and G. L. Stephens (2007), A multipurpose radar simulation package: QuickBeam, *Bull. Am. Meteorol. Soc.*, **88**, 1723–1727, doi:10.1175/BAMS-88-11-1723.

Jakob, C. (2003), An Improved Strategy for the Evaluation of Cloud Parameterizations in GCMS. *Bull. Amer. Meteor. Soc.,* **84**, 1387–1401, doi: 10.1175/BAMS-84-10-1387.

Jakob, C., and G. Tselioudis (2003), Objective identification of cloud regimes in the Tropical Western Pacific, Geophys. Res. Lett., **30**, 2082, doi:10.1029/2003GL018367, 21.

Jiang, J. H., et al. (2015), Evaluating the diurnal cycle of upper tropospheric ice clouds in climate models using SMILES observations, *J. Atmos. Sci.*, **72**, 1022–1044.

Jiang, Peng, et al. (2016), Changes of storm properties in the United States: Observations and multimodel ensemble projections. *Global and Planetary Change* **142**, 41-52.

Jiang, X., N.-C. Lau, and S. A. Klein (2006), Role of eastward propagating convection systems in the diurnal cycle and seasonal mean of summertime rainfall over the U.S. Great Plains, *Geophys. Res. Lett*., **33**, L19809, doi:10.1029/2006GL027022.

Kennedy, A., X. Dong, and B. Xi (2015), Cloud fraction at the ARM SGP site: Reducing uncertainty with self organizing maps, *Theor. Appl. Climatol.*, **124**, 43, doi:10.1007/s00704-015-1384-3.

Kollias, P., G. Tselioudis, and B. A. Albrecht (2007), Cloud climatology at the Southern Great Plains and the layer structure, drizzle, and atmospheric modes of continental stratus, *J. Geophys. Res.*, **112**, D09116, doi:10.1029/2006JD007307.

Kollias, P., E. E. Clothiaux, et al. (2016), Development and applications of ARM millimeter-wavelength cloud radars, Meteorol. Monogr., 57, 17.1–17.19, doi:10.1175/AMSMONOGRAPHS-D-15-0037.1.

Khairoutdinov, M. F., and D. A. Randall (2003), Cloud resolving modeling of the ARM summer 1997 IOP: Model formulation, results, uncertainties, and sensitivities, *J. Atmos. Sci.*, **60**, 607–625, doi:10.1175/1520-0469(2003)060<0607:CRMOTA>2.0.CO;2.

Khairoutdinov, M., D. Randall, and C. DeMott (2005), Simulations of the atmospheric general circulation using a cloud-resolving model as a superparameterization of physical processes, *J. Atmos. Sci.*, **62**(7), 2136–2154.

Khairoutdinov, M., C. Demott, and D. Randall (2008), Evaluation of the simulated interannual and subseasonal variability in an AMIP-style simulation using the CSU multiscale modeling framework, *J. Clim.*, **21**, 413–431.

Klein, S. A., Y. Zhang, M. D. Zelinka, R. Pincus, J. Boyle, and P. J. Gleckler (2013), Are climate model simulations of clouds improving? An evaluation using the ISCCP simulator, *J. Geophys. Res. Atmos.*, **118**, 1329–1342, doi:10.1002/jgrd.50141.

Kuang, Z., and C. S. Bretherton (2006), A mass-flux scheme view of a high-resolution simulation of a transition from shallow to deep convection, *J. Atmos. Sci.*, **63**, 1895–1909.

Lazarus, S. M., S. K. Krueger, and G. G. Mace (2000), A cloud climatology of the Southern Great Plains ARM CART, *J. Clim.*, **13**, 1762–1775.

Lee, M.-I., I. Choi, W.-K. Tao, S. D. Schubert, and I.-K. Kang (2010), Mechanisms of diurnal precipitation over the United States Great Plains: A cloud-resolving model simulation, *Clim. Dyn.*, **34**, 419–437.

Lin, W., Y. Liu, A. M. Vogelmann, A. Fridlind, S. Endo, H. Song, S. Feng, T. Toto, Z. Li, and M. Zhang (2015), RACORO continental boundary layer cloud investigations: 3. Separation of parameterization biases single-column model CAM5 simulations of shallow cumulus. *J. Geophys. Res. Atmos.*, **120**, 6015–6033. doi: 10.1002/2014JD022524.

Liu, C., and E. J. Zipser (2008), Diurnal cycles of precipitation, clouds, and lightning in the tropics from 9 years of TRMM observations, *Geophys. Res. Lett*., **35**, L04819, doi:10.1029/2007GL032437.

Liu, Y., B. Geerts, M. Miller, P. Daum, and R. McGraw (2008), Threshold radar reflectivity for drizzling clouds, Geophys. Res. Lett., 35, L03807, doi:10.1029/2007GL031201.

Liu, Z., A. Muhlbauer, and T. Ackerman (2015), Evaluation of high-level clouds in cloud resolving model simulations with ARM and KWAJEX observations*, J. Adv. Model. Earth Syst.*, **7**, 1716–1740, doi:10.1002/2015MS000478.

Luo, Z., and G. L. Stephens (2006), An enhanced convection-wind-evaporation feedback in a superparameterization GCM (SP-GCM) depiction of the Asian summer monsoon, *Geophys. Res. Lett.*, **33**, L06707, doi:10.1029/2005GL025060.

Mace, G. G., and K. Sassen (2000), A constrained algorithm for retrieval of stratocumulus cloud properties using solar radiation, microwave radiometer, and millimeter cloud radar data, *J. Geophys. Res.*, **105**, 29, 099–29,108.

Marchand, R. T., N. Beagley, S. Thompson, T. P. Ackerman, and D. M. Schultz (2006), A bootstrap technique for testing the relationship between local-scale radar observations of cloud occurrence and large-scale atmospheric fields, *J. Atmos. Sci.*, **63**(11), 2813–2830, doi:10.1175/JAS3772.1.

Marchand, R., J. Haynes, G. G. Mace, T. Ackerman, and G. Stephens (2009a), A comparison of simulated cloud radar output from the multiscale modeling framework global climate model with CloudSat cloud radar observations, *J. Geophys. Res*., **114**, D00A20, doi:10.1029/2008JD009790.

Marchand, R., N. Beagley, and T. P. Ackerman (2009b), Evaluation of hydrometeor occurrence profiles in the multiscale modeling framework climate model using atmospheric classification, *J. Clim.*, **22**, 4557–4573, doi:10.1175/2009JCLI2638.1.

Marchand, R., and T. Ackerman (2010), An analysis of cloud cover in multiscale modeling framework global climate model simulations using 4 and 1 km horizontal grids, *J. Geophys. Res.*, **115**, D16207, doi:10.1029/2009JD013423.

McFarlane, S. A., J. H. Mather, and T. P. Ackerman (2007), Analysis of tropical radiative heating profiles: A comparison of models and observations, *J. Geophys. Res.*, **112**, D14218, doi:10.1029/2006JD008290.

Moran, K. P., B. E. Martner, M. J. Post, R. A. Kropfli, D. C. Welsh, and K. B. Widener (1998), An unattended cloud-profiling radar for use in climate research, *Bull. Am. Meteorol. Soc.*, **79**, 443–455.

Nesbitt, S. and E. Zipser (2003): The Diurnal Cycle of Rainfall and Convective Intensity according to Three Years of TRMM Measurements. *J. Climate,* **16**, 1456–1475, doi: 10.1175/1520-0442(2003)016<1456:TDCORA>2.0.CO;2.

Nesbitt S, Gochis D, Lang T. (2008), The diurnal cycle of clouds and precipitation along the Sierra Madre occidental observed during NAME-2004: implications for warm season precipitation estimation in complex terrain. *J. Hydrometeorol.* **9**: 728–743.

Norris, J. and C. Weaver (2001): Improved Techniques for Evaluating GCM Cloudiness Applied to the NCAR CCM3. *J. Climate,* **14**, 2540–2550, doi: 10.1175/1520-0442(2001)014<2540:ITFEGC>2.0.CO;2.

Pritchard, M. S., and R. C. J. Somerville (2009a), Assessing the Diurnal Cycle of Precipitation in a Multi-Scale Climate Model, *J. Adv. Model. Earth Syst*., **1**, 12, doi:10.3894/JAMES.2009.1.12.

Pritchard, M. S., and R. C. J. Somerville (2009b), Empirical orthogonal function analysis of the diurnal cycle of precipitation in a multi-scale climate model, *Geophys. Res. Lett*., **36**, L05812, doi:10.1029/2008GL036964.

Pritchard, M. S., M. W. Moncrieff, and R. C. J. Somerville (2011), Orogenic propagating precipitation systems over the United States in a global climate model with embedded explicit convection, *J. Atmos. Sci.*, **68**, 1821–1840.

Randall, D., M. Khairoutdinov, A. Arakawa, and W. Grabowski (2003), Breaking the cloud parameterization deadlock, *Bull. Am. Meteorol. Soc.*, **84**, 1547–1564.

Shafer, M., D. Ojima, J. M. Antle, D. Kluck, R. A. McPherson, S. Petersen, B. Scanlon, and K. Sherman (2014): Ch. 19: Great Plains. Climate Change Impacts in the United States: The Third National Climate Assessment, J. M. Melillo, Terese (T.C.) Richmond, and G. W. Yohe, Eds., U.S. Global Change Research Program, 441-461.

Stephens, G. L., T. L'Ecuyer, R. Forbes, A. Gettlemen, J.-C. Golaz, A. Bodas-Salcedo, K. Suzuki, P. Gabriel, and J. Haynes (2010), Dreary state of precipitation in global models, *J. Geophys. Res.*, **115**, D24211, doi:10.1029/2010JD014532.

Stevens, B., and J.-L. Brenguier (2009), Cloud controlling factors: Low clouds, in *Clouds in the Perturbed Climate System*, edited by J. Heintzenberg, and R. J. Charlson, pp. 173–196, MIT Press, Cambridge, Mass.

Tian, B., B. J. Soden, and X. Wu (2004), Diurnal cycle of convection, clouds, and water vapor in the tropical upper troposphere: Satellites versus a general circulation model, *J. Geophys. Res.*, **109**, D10101, doi:10.1029/2003JD004117.

Tselioudis, G., Y. Zhang, and W. Rossow (2000), Cloud and Radiation Variations Associated with Northern Midlatitude Low and High Sea Level Pressure Regimes. *J. Clim.,* **13**, 312–327, doi: 10.1175/1520-0442(2000)013<0312:CARVAW>2.0.CO;2.

Tselioudis, G., and C. Jakob (2002), Evaluation of midlatitude cloud properties in a weather and a climate model: Dependence on dynamic regime and spatial resolution, *J. Geophys. Res.*, **107**(D24), 4781, doi:10.1029/2002JD002259.

Trenberth, K. E. (2011), Changes in precipitation with climate change, *Clim. Res.*, **47**, 123–138, doi:10.3354/cr00953.

Wallace, J. M. (1975), Diurnal variations in precipitation and thunderstorm frequency over the conterminous United States, *Mon. Weather Rev.*, **103**, 406–419.

Wang, M., V. E. Larson, S. Ghan, M. Ovchinnikov, D. P. Schanen, H. Xiao, X. Liu, P. Rasch, and Z. Guo (2015), A multiscale modeling framework model (superparameterized CAM5) with a higher-order turbulence closure: Model description and low-cloud simulations, *J. Adv. Model. Earth Syst.*, **7**, 484–509, doi:10.1002/2014MS000375.

Wyant, M. C., C. S. Bretherton, and P. N. Blossey (2009), Subtropical Low Cloud Response to a Warmer Climate in a Superparameterized Climate Model. Part I: Regime Sorting and Physical Mechanisms, J. Adv. Model. Earth Syst., 1, 7, doi:10.3894/JAMES.2009.1.7.

Xu, W. and E. Zipser (2011): Diurnal Variations of Precipitation, Deep Convection, and Lightning over and East of the Eastern Tibetan Plateau. *J. Clim.,* **24**, 448–465, doi: 10.1175/2010JCLI3719.1.

Yuan, J., Q. Fu, and N. McFarlane (2006), Tests and improvements of GCM cloud parameterizations using the CCCMA SCM with the SHEBA data set. *Atmos. Res.* **82**: 222–238.

Zhang, G., K. Cook, and E. Vizy, 2016: The Diurnal Cycle of Warm Season Rainfall over West Africa. Part I: Observational Analysis. *J. Clim.,* **29**, 8423–8437, doi: 10.1175/JCLI-D-15-0874.1.

Zhang, Y., and S. A. Klein (2010), Mechanisms affecting the transition from shallow to deep convection over land: inferences from observations of the diurnal cycle collected at the ARM Southern Great Plains Site. *J. Atmos. Sci.* **67**: 2943–2959.

Zhang, Y., S. A. Klein, C. Liu, B. Tian, R. T. Marchand, J. M. Haynes, R. B. McCoy, Y. Zhang, and T. P. Ackerman (2008), On the diurnal cycle of deep convection, high-level cloud, and upper troposphere water vapor in the Multiscale Modeling Framework, *J. Geophys. Res*., **113**, D16105, doi:10.1029/2008JD009905.